

MODELDIFF: A Framework for Comparing Learning Algorithms

Harshay Shah*, Sung Min Park*, Andrew Ilyas*, Aleksander Madry
{[harshay](mailto:harshay@mit.edu), [sp765](mailto:sp765@mit.edu), [ailyas](mailto:ailyas@mit.edu), [madry](mailto:madry@mit.edu)}@mit.edu
Massachusetts Institute of Technology

Abstract

We study the problem of *(learning) algorithm comparison*, where the goal is to find differences between models trained with two different learning algorithms. We begin by formalizing this goal as one of finding *distinguishing feature transformations*, i.e., input transformations that change the predictions of models trained with one learning algorithm but not the other. We then present MODELDIFF, a method that leverages the datamodels framework [IPE+22] to compare learning algorithms based on how they use their training data. We demonstrate MODELDIFF through three case studies, comparing models trained with/without data augmentation, with/without pre-training, and with different SGD hyperparameters. Our code is available at <https://github.com/MadryLab/modeldiff>.

*Equal contribution.

1 Introduction

Building a machine learning model involves making a number of design choices. Indeed, even after choosing a dataset, one must decide on a model architecture, an optimization method, and a data augmentation pipeline. It is these design choices together that define the *learning algorithm*, i.e., the function mapping training datasets to machine learning models.

One of the key reasons why these design choices matter to us is that—even when they do not directly affect accuracy—they determine the *biases* of the resulting models. For example, Hermann et al. [HCK20] find significant variation in shape bias [GRM+19] across a group of ImageNet models that vary in accuracy by less than 1%. Similarly, Liu et al. [LXL+22] find that language models with the same loss can have drastically different implicit biases and as a result, different performances when used for transfer learning.

Motivated by this, we develop a framework for comparing learning algorithms. Our framework is *general* in the sense that one can use it to study *any* pair of algorithms *without* a prior hypothesis on what the difference between them is. As a result, it enables us to precisely dissect the impact of particular design choices. Specifically, our two main contributions are:

- (a) **A precise, quantitative definition of the algorithm comparison problem.** We introduce the problem of (*feature-based*) *learning algorithm comparison*. Given two learning algorithms, the (intuitive) goal here is to find features used by one learning algorithm but not by the other. We formalize this goal by stating it as one of finding transformations in input space that induce different behavior from (i.e., that *distinguish*) models trained by the two learning algorithms (Section 2.1).
- (b) **A method for comparing any two algorithms.** We propose a method, MODELDIFF, for comparing algorithms in terms of *how they use the training data*. The key tool we leverage here is *datamodeling* [IPE+22], which allows us to quantify the impact of each training example on a specific (single) model prediction (see Section 2.2). Intuitively, two models that use different features to arrive at their final predictions should differ in what training examples they rely on¹. We translate this intuition into a method with formal guarantees in Section 3. The output of our method is a set of *distinguishing subpopulations*, groups of test examples for which the two algorithms systematically differ in *how* they make predictions.

We tie our method (b) back to our formal definition of algorithm comparison in (a) by looking for a pattern within each distinguishing subpopulation, and using it to design a candidate input transformation (Figure 1 middle). We then “verify” this transformation (Figure 1 right) through counterfactual analysis.

We illustrate the utility of our framework through three case studies (Section 4), which are motivated by typical choices one needs to make within machine learning pipelines, namely:

- **Data augmentation:** We compare classifiers trained with and without data augmentation on the LIVING17 [STM21] dataset. We show that models trained with data augmentation are more prone to picking up instances of co-occurrence bias and texture bias compared to models trained without data augmentation. For instance, adding a spider web to random images increases the “spider” confidence of models trained with (without) augmentation by 15% (1%) on average.

¹For example, suppose we were comparing a texture-biased model to a shape-biased one: when faced with a test example containing, e.g., a cat in a unique pose, the texture-biased model will rely on examples from the training set with similar texture (e.g., fur), whereas the shape-biased model will rely more on examples in a similar pose.

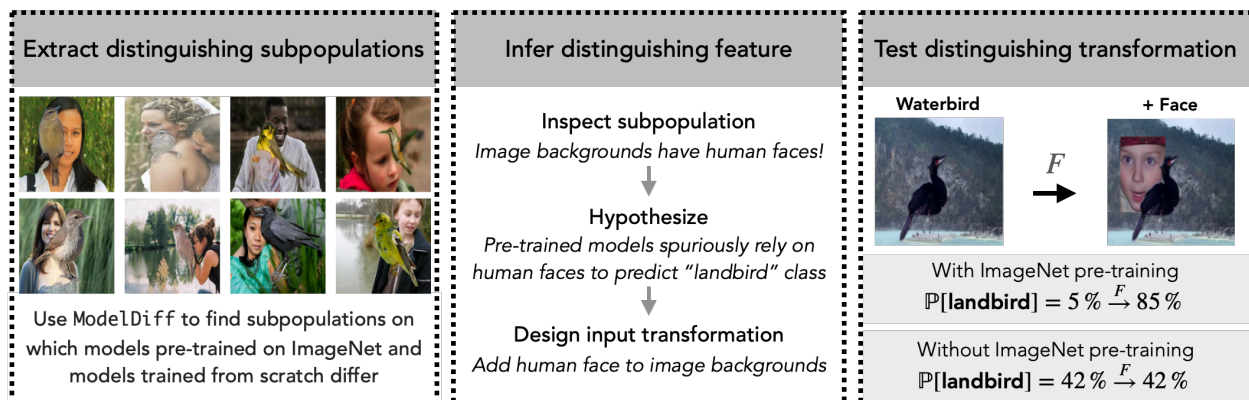


Figure 1: A demonstration of our approach. Our method (Section 3) automatically extracts coherent subpopulations of images (left) on which models differ in terms of what features they use. Then, an interpreter—whether human or automated—uses these subpopulations to design a *feature transformation* that they think will distinguish the models (middle). Finally, we verify the validity of this feature transformation via counterfactual analysis (right).

- **ImageNet pre-training:** We compare classifiers first pre-trained on ImageNet [DDS+09; RDS+15] then fine-tuned on WATERBIRDS task [SKH+20] to classifiers trained from scratch on WATERBIRDS. We demonstrate that pre-training can either suppress or amplify specific spurious correlations. For example, adding a yellow patch to random images changes models’ average confidence in the “landbird” label by +12% (-4%) when training from scratch (pre-training) . Meanwhile, adding a human face to the background changes the “landbird” confidence of pre-trained (from-scratch) models by +4% (-1%).
- **SGD hyperparameters:** Finally, we compare classifiers trained on CIFAR-10 [Kri09] with different choices of learning rates and batch sizes. Our analysis pinpoints subtle differences in model behavior induced by small changes to these hyperparameters. For example, adding a small pattern that resembles windows to random images increases the “truck” confidence by 7% on average for models trained with a smaller learning rate, but increases the confidence by only 2% for models trained with a larger learning rate.

Across all three case studies, our framework surfaces fine-grained differences between models trained with different learning algorithms, enabling us to better understand the role of the design choices that make up a learning algorithm.

2 Preliminaries and Setup

We begin by laying the groundwork for both our formalization of algorithm comparison as well as our proposed approach. In Section 2.1, we state the algorithm comparison problem, and formalize it as the task of identifying *distinguishing transformations*. These are functions that—when applied to test examples—significantly and consistently change the predictions of one model class but not the other. In Section 2.2, we introduce *datamodels* [IPE+22], the key primitive behind our approach to algorithm comparison (which we present in Section 3).

2.1 Formalizing algorithm comparisons via distinguishing transformations

The goal of algorithm comparison problem is to understand the ways in which two learning algorithms (trained on the same dataset) differ in the models they yield. More specifically, we are interested in comparing the *model classes* induced by the two learning algorithms:

Definition 1 (Induced model class). *Given an input space \mathcal{X} , a label space \mathcal{Y} , and a model space $\mathcal{M} \subset \mathcal{X} \rightarrow \mathcal{Y}$, a learning algorithm $\mathcal{A} : (\mathcal{X} \times \mathcal{Y})^* \rightarrow \mathcal{M}$ is a (potentially random) function mapping a set of input-label pairs to a model. Fixing a data distribution \mathcal{D} , the model class induced by algorithm \mathcal{A} is the distribution over \mathcal{M} that results from applying \mathcal{A} to randomly sampled datasets from \mathcal{D} .*

Focusing on model classes (rather than individual models) isolates differences induced by the learning algorithms themselves rather than by any inherent non-determinism in training [ZGK+21; DHM+20; JNB+21]. The perspective we adopt here is that model classes differ insofar as they use different features to make predictions. Thus, our goal when comparing two algorithms should be to pinpoint features that one model class uses but the other does not. Rather than try to precisely define “feature,” however, we make this notion precise by defining functions that we call *distinguishing (feature) transformations*:

Definition 2 (Distinguishing transformation). *Let $\mathcal{A}_1, \mathcal{A}_2$ denote learning algorithms, S a dataset of input-label pairs, and \mathcal{L} a loss function (e.g., correct-class margin). Suppose M_1 and M_2 are models trained on dataset \mathcal{D} using algorithms \mathcal{A}_1 and \mathcal{A}_2 respectively. Then, a (ϵ, δ) -distinguishing feature transformation of M_1 with respect to M_2 is a function $F : \mathcal{X} \rightarrow \mathcal{X}$ such that for some label $y_c \in \mathcal{Y}$,*

$$\overbrace{\mathbb{E}[L_1(F(x), y_c) - L_1(x, y_c)]}^{\text{Counterfactual effect of } F \text{ on } M_1} \geq \delta \quad \text{and} \quad \overbrace{\mathbb{E}[L_2(F(x), y_c) - L_2(x, y_c)]}^{\text{Counterfactual effect of } F \text{ on } M_2} \leq \epsilon,$$

where $L_i(x, y) = \mathcal{L}(M_i(x), y)$ is the loss of a model trained with algorithm i on the pair (x, y) , and the expectations above are taken over inputs x and randomness in the learning algorithm.

Intuitively, a distinguishing feature transformation is just a function F that, when applied to test examples, significantly changes the predictions of one model class—but not the other—in a consistent way. Definition 2 also immediately suggests a way to *evaluate* the effectiveness of a distinguishing feature transformation. That is, given a hypothesis about how two algorithms differ (e.g., that models trained with \mathcal{A}_1 are more sensitive to texture than those trained with \mathcal{A}_2), one can design a corresponding transformation F (e.g., applying style transfer, as in [GRM+19]), and directly measure its relative effect on the two model classes.

Informative distinguishing transformations (IDTs). Not every distinguishing transformation F sheds the same amount of light on model behavior. For example, given any two non-identical learning algorithms, we could craft a transformation F that imperceptibly modifies its input to satisfy Definition 2 (e.g., by using adversarial examples). Alternatively, one could craft an F that arbitrarily transforms its inputs into pathological out-of-distribution examples on which the two model classes disagree. While these transformations satisfy Definition 2, they yield no benefit in terms of qualitatively understanding the differences in *salient* features used by the model classes. More concretely, an *informative* distinguishing feature transformation must (a) capture a feature that naturally arises in the data distribution and (b) be semantically meaningful.

2.2 Datamodel representations for comparison

Before presenting our approach to comparing learning algorithms (Section 3), we provide an overview of the underlying datamodeling framework [IPE+22], and its applicability to learning algorithm comparison.

A primer on datamodels. Let us fix a learning algorithm \mathcal{A} (i.e., a map from training datasets to machine learning models), a training set $S = \{x_1, \dots, x_d\}$, and a *specific* test example $x \in T$. For any subset $S' \subset S$ of the training set, we follow [IPE+22] and define the *model output function*

$$f(x, S') = \text{the loss after training a model on } S' \text{ (using } \mathcal{A} \text{) and evaluating on } x. \quad (1)$$

Ilyas et al. [IPE+22] show that one can often approximate the model output function above with a much simpler model, which they call a *datamodel*. For example, if the learning algorithm \mathcal{A} is training a neural network on a standard image classification task and the output function f is the *correct-class margin* of the resulting classifier, a simple *linear* predictor suffices, i.e.,

$$\mathbb{E}[f(x, S')] \approx \theta_x \cdot \mathbf{1}_{S'}, \quad (2)$$

where θ_x is a (learned) parameter vector and $\mathbf{1}_{S'} \in \{0, 1\}^{|S|}$ is a binary *indicator vector* of the set S' , encoding whether each example of S is included in S' , i.e.,

$$(\mathbf{1}_{S'})_i = \mathbb{1}\{x_i \in S'\}.$$

The vector θ_x is called the *datamodel* for the example x , and one can compute it by sampling a collection of random subsets $S_k \subset S$, training a model on each subset, and solving a (regularized) linear regression problem of predicting $f(x, S_k)$ from $\mathbf{1}_{S_k}$, i.e.,

$$\theta_x = \arg \min_{\theta} \sum_{k=1}^n \left(f(x, S_k) - \theta_x^\top \mathbf{1}_{S_k} \right)^2 + \lambda_x \|\theta\|_1,$$

where cross-validation determines the regularization strength $\lambda_x \in \mathbb{R}$. Together, the resulting datamodel vectors for each test example form the *datamodel matrix* $\Theta \in \mathbb{R}^{|T| \times |S|}$.

Datamodel representations. For our purposes, it will be convenient to view the datamodel θ_j for a test example x_j as a $|S|$ -dimensional *representation* of x_j , where the i -th coordinate θ_{ji} of this representation is the extent to which models trained with \mathcal{A} rely² on the i -th training example to classify example x_j . These representations have two properties that make them a useful tool for model comparison:

- (a) **Consistent basis:** The i -th coordinate of a datamodel representation always corresponds to the importance of the i -th training example, making datamodels inherently comparable across learning algorithms (as long as the training set is fixed). In other words, datamodel representations are *automatically aligned* across different algorithms, and even across models that lack explicit representations (e.g., decision trees).
- (b) **Predictiveness:** Datamodels have a natural *causal* interpretation. In particular, Ilyas et al. [IPE+22] show that datamodels can predict the counterfactual effect of removing or adding different training examples on model output for a given test example. As a result, any trends we find across the datamodel representations come with a precise quantitative interpretation in terms of model outputs (we return to this point in Section 3).

²For readers familiar with influence functions [KL17; HRR+11], an intuitive (but not quite accurate) way to interpret the datamodel weight θ_{ji} is as the influence of the i -th training example on test example x_j .

3 Comparing learning algorithms with MODELDIFF

Recall (from Section 2.1) that we want to identify informative distinguishing transformations (IDTs). These are functions in input space that (a) induce different behavior from the two learning algorithms being studied; while (b) capturing a feature that arises naturally in the data and (c) being semantically meaningful. Now, both the size of the space of transformations as well as the subjective nature of “semantically meaningful” make it futile to search for IDTs directly.

Instead, our method (called MODELDIFF) outputs a set of *distinguishing subpopulations*, groups of examples with a common feature that is used by one learning algorithm and not the other. One can use these subpopulations to design IDTs, whether by inspection or domain-specific analysis. MODELDIFF finds these subpopulations by examining *how each algorithm uses the training data*, and comprises the following steps:

Step 1: Compute normalized datamodels for each algorithm. We start by computing a datamodel representation [IPE+22] for each example in the test set T . Specifically, we compute two sets of datamodels— $\Theta^{(1)}, \Theta^{(2)} \in \mathbb{R}^{|T| \times |S|}$ —corresponding to the model classes induced by learning algorithms \mathcal{A}_1 and \mathcal{A}_2 respectively. After computing the datamodels, we *normalize* each one—that is, we divide each datamodel (or equivalently, each row of $\Theta^{(i)}$) by its ℓ_2 norm.

Step 2: Compute residual datamodels. Next, we compute a *residual datamodel* for each test example x_i , which is the projection of the datamodel $\theta_i^{(1)}$ onto the null space of datamodel $\theta_i^{(2)}$:

$$\theta_i^{(1\setminus 2)} = \theta_i^{(1)} - \text{proj}_{\theta_i^{(2)}}(\theta_i^{(1)}). \quad (3)$$

Intuitively, the residual datamodels of algorithm \mathcal{A}_1 with respect to \mathcal{A}_2 correspond to the training directions that influence \mathcal{A}_1 after “projecting away” the component that also influences \mathcal{A}_2 .

Step 3(i): Run PCA on residual datamodels. Finally, we use principal component analysis to find the highest-variance directions in the space of residual datamodels. That is, we run

$$\ell\text{-PCA}(\{\theta_1^{(1\setminus 2)}, \dots, \theta_{|T|}^{(1\setminus 2)}\}) \quad (4)$$

to find the top ℓ principal components $\{u_1, \dots, u_\ell\}$ of the residual datamodels. Intuitively, these principal components—which we call *distinguishing training directions*—correspond to (weighted) combinations of training examples that together are used by one algorithm and not the other.

How do we verify that these principal components actually help us distinguish the two learning algorithms? Proposition 1 below leverages the predictive properties of datamodels to establish that connection. Specifically, it shows that for a training direction to truly distinguish \mathcal{A}_1 from \mathcal{A}_2 (in terms of model behavior), it suffices to explain a high (resp., low) amount of the variance in datamodel representations of algorithm \mathcal{A}_1 (resp., \mathcal{A}_2). Importantly, the latter conditions can be checked directly by simply plotting the explained variances of each component—see Figure 2(3i).

Proposition 1 (Informal—see Appendix A for a formal statement and proof). *Assume for illustrative purposes that Eq. (2) holds with equality (i.e., that datamodels perfectly approximate model output). Let $\mathbf{u} \in \mathbb{R}^{|S|}$ be a principal component identified in (4), and define the explained variance gap as*

$$\Delta(\mathbf{u}) = \|\Theta^{(1)}\mathbf{u}\|^2 - \|\Theta^{(2)}\mathbf{u}\|^2.$$

Then, up/down-weighting the training set S (in a specific way) according to \mathbf{u} will change outputs of algorithm \mathcal{A}_1 by $\Delta(\mathbf{u})$ more than the outputs of algorithm \mathcal{A}_2 on average (i.e., across test examples).

Step 3(ii): From principal components to subpopulations. We now have a set of ℓ distinguishing training directions u_i (i.e., principal components of the residual datamodel matrix) that we have verified by measuring $\Delta(u)$ from Proposition 1. The final step in our method is to translate each distinguishing direction u_i into a corresponding *distinguishing subpopulation*, i.e., the set of test examples x_j whose residual datamodels $\theta_j^{(1/2)}$ most closely align with u_i (See Figure 2(3ii)).

Connecting back to our algorithm comparison objective. The output of MODELDIFF is the set of distinguishing subpopulations from Step 3(ii). We connect these subpopulations back to our formal definition of the comparison problem (Definition 2) by inferring a *distinguishing feature* for each one³ (e.g., in Figure 2, all the images in the distinguishing subpopulation have an orange tint). We then design a transformation that adds this feature to inputs (e.g., adding an orange tint—Figure 2(4)), and measure its average effect on models trained with \mathcal{A}_1 and \mathcal{A}_2 .

We illustrate our end-to-end process (including the verification step) visually in Figure 2.

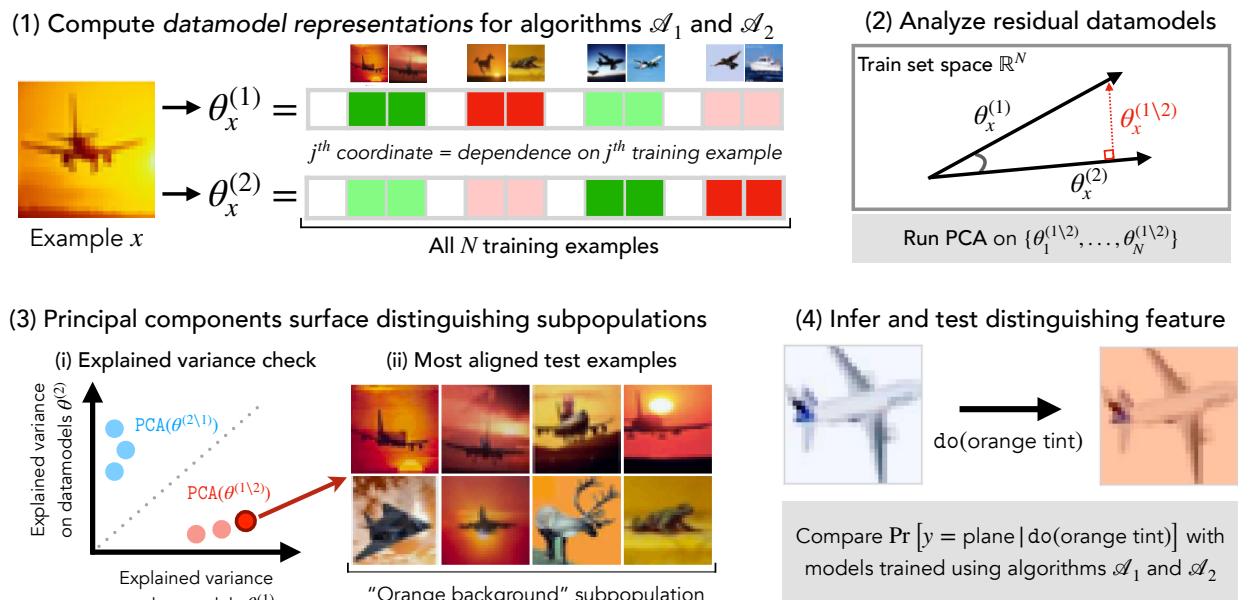


Figure 2: A visual summary of our approach. We (1) compute datamodel representations for each algorithm [IPE+22], then (2) compute residual datamodels (3); next, (3) PCA on these residual datamodels yields so-called “distinguishing subpopulations.” Finally, in (4) simple inspection suffices to turn this subpopulation into a feature transformation that we test with Definition 2.

4 Case studies: Applying MODELDIFF

We demonstrate our comparison framework using three case studies that each study a key aspect of the standard training pipeline—namely, data augmentation, pre-training, and optimizer. In each case study, we follow the same procedure: (i) we use the MODELDIFF algorithm from Section 3 above to identify *distinguishing subpopulations*; (ii) we inspect these subpopulations to come up with a *candidate distinguishing transformation*; and (iii) we apply these candidate transformation to test examples and compare its effect on models trained with the two learning algorithms.

³We intentionally leave this step open-ended to ensure our method is applicable across domains and modalities. In vision specifically, we can streamline this step using text-vision models like CLIP [RKH+21] (see Appendix F.5).

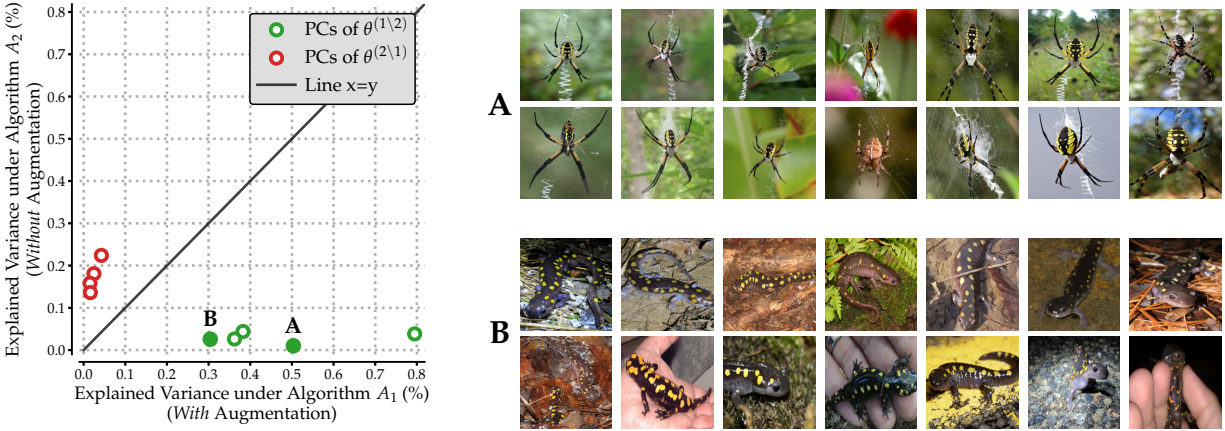


Figure 3: **Comparing LIVING17 models trained with and without standard data augmentation.** (Left) Each green (resp., red) point is a *training direction* (i.e., a vector $v \in \mathbb{R}^{|S|}$ representing a weighted combination of training examples) that distinguishes \mathcal{A}_1 from \mathcal{A}_2 (resp., \mathcal{A}_2 from \mathcal{A}_1) as identified by MODELDIFF (i.e., each point is a solution to (4)). The x and y coordinates of each point represent the “importance” (as given by Proposition 1) of the training direction to models trained with \mathcal{A}_1 and \mathcal{A}_2 respectively. (Right) The surfaced distinguishing subpopulations, corresponding to the distinguishing training directions annotated **A** and **B**. Direction **A** surfaces spiders on spider webs, and direction **B** surfaces salamanders with yellow polka dots.

4.1 Case study: Data augmentation

Data augmentation is a key component of the standard computer vision training pipeline. Still, while it often improves overall performance, the effect of data augmentation on models’ learned *features* remains elusive. In this case study, we study the effect of data augmentation on classifiers trained for the ImageNet-derived LIVING17 task [STM21]. Specifically, we compare two classes of ResNet-18 models trained on this dataset with the exact same settings modulo the use of data augmentation, i.e.,

- **Algorithm \mathcal{A}_1 :** Training with standard augmentation, (namely, horizontal flip and resized random crop with torchvision default parameters). Resulting models attain 89% average test accuracy (where the average is taken over randomness in training).
- **Algorithm \mathcal{A}_2 :** Training without data augmentation. Models attain 81% average accuracy.

Appendix B.1 provides further experimental details for this case studies and the others.

Applying MODELDIFF. Applying our MODELDIFF method to algorithms \mathcal{A}_1 and \mathcal{A}_2 gives us a set of distinguishing subpopulations, visualized in Figure 3 (right).

On the left side of the same figure—inspired by Proposition 1—we plot the variance explained by each distinguishing training direction (i.e., the solutions to (4)) in the datamodels for both \mathcal{A}_1 (x axis) and \mathcal{A}_2 (y axis). The training directions distinguishing \mathcal{A}_1 from \mathcal{A}_2 (in green) indeed explain a significant amount of variance in the datamodels of \mathcal{A}_1 but not in those of \mathcal{A}_2 . For the directions distinguishing \mathcal{A}_2 from \mathcal{A}_1 (in red) the situation is reversed, just as we would expect.

From subpopulations to IDTs. The subpopulations in Figure 3 suggest the following features:

- **Spider web:** Direction **A** surfaces a subpopulation of test images that contain spiders. In contrast to random spider images in LIVING17, all the images in the surfaced subpopulation contain a *spider web* in the background (Appendix D). We thus hypothesize that models trained with standard data augmentation—more so than those trained without it—use spider webs to predict the class “spider”. We test this hypothesis using a feature transformation that overlays a spider web pattern onto an entire image (see Figure 4a).
- **Polka dots:** Direction **B** surfaces a subpopulation of test images that contain salamanders. Again, comparing these images to random salamander images in LIVING17 test data reveals yellow-black polka dots as a common feature (see also Appendix D). This suggests that models trained with data augmentation might rely on the polka dot texture to predict the class “salamander.” To test this hypothesis, we design a feature transformation that adds small yellow polka dots to the entire image (see Figure 4b).

We provide additional analysis in support of these hypotheses in Appendix D.

Figure 4 shows the effect of the above transformations on models trained with and without data augmentation. The results confirm our hypotheses. For example, overlaying a spider web pattern with 30% opacity increases $P(\text{“spider”})$ (i.e., models’ average softmax confidence in the spider label) for models trained with (without) data augmentation by 11% (1%). Similarly, overlaying the yellow polka dot texture with 30% opacity increased $P(\text{“salamander”})$ by 14% (2%). Furthermore, increasing the transformations’ intensity consistently widens the gap between the predictions of the two model classes. Overall, these differences verify that the feature transformations we constructed can indeed distinguish the two learning algorithms as per Definition 2.

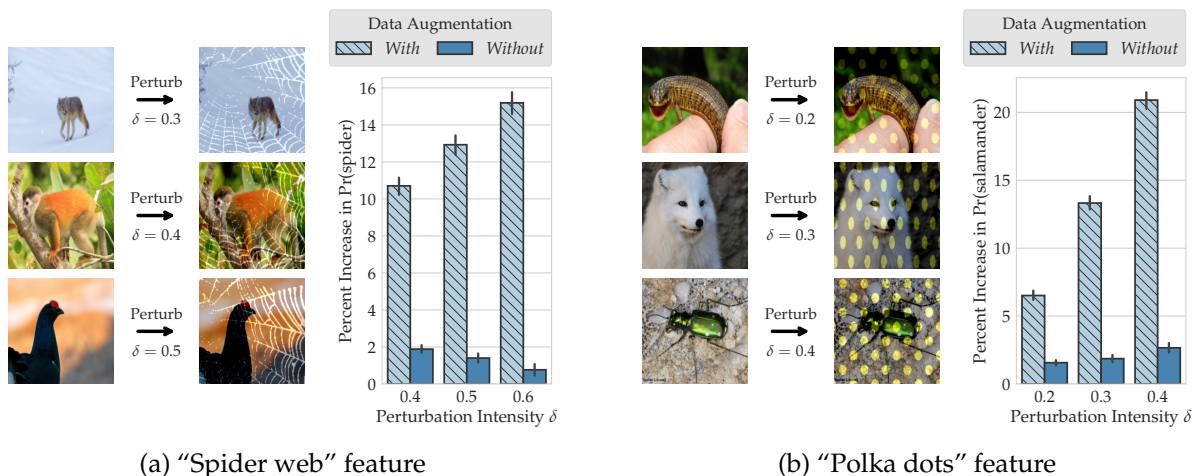


Figure 4: **Effect of data augmentation on LIVING17 models.** Standard data augmentation amplifies specific instances of co-occurrence (panel (a)) and texture (panel (b)) biases. The left side of each panel illustrates the distinguishing feature transformation at three different intensities δ . On the right, we plot the average effect of the transformation on the confidence of models trained with and without data augmentation, for varying δ . At moderate intensity δ , adding a spider web pattern to images makes models trained with (without) data augmentation, on average, 13% (1%) more confident in predicting the class “spider,” while overlaying a polka dot pattern makes them 14% (2%) more confident in the class “salamander.” In both cases, increasing the intensity δ widens the gap between the two model classes.

Connection to previous work. Our case study demonstrates how training with standard data augmentation on LIVING17 data can amplify specific instances of co-occurrence bias (spider webs) and texture bias (polka dots). These findings are consistent with prior works that show that data augmentation can introduce biases (e.g., [HCK20]). Also, the distinguishing features that we find are specific to certain classes—this may explain why data augmentation can have disparate impacts on performance across different classes [BBL22]. Finally, our findings, which demonstrate how data augmentation alters relative importance of specific features, corroborate the view of data augmentation as *feature manipulation* [SBG22].

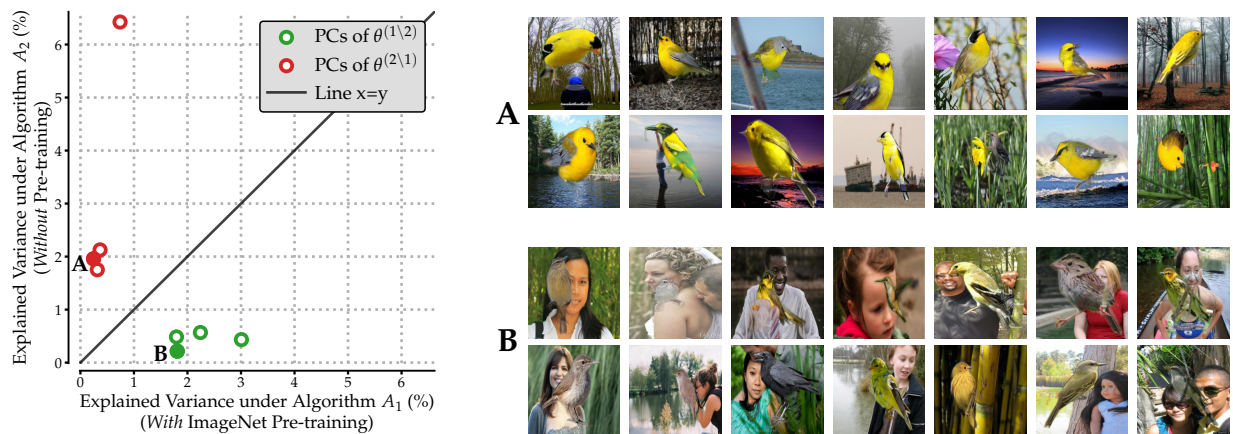


Figure 5: **Comparing Waterbirds models trained with and without ImageNet pre-training.** An analog to Figure 3 for our second case study, see Figure 3 for a description. In this case, subpopulation A seems to correspond to yellow birds and subpopulation B to faces in the background.

4.2 Case study: Pre-training

Pre-training on large datasets is a standard approach to improving performance on downstream tasks where training data is scarce. In this case study, we study the effect of ImageNet pre-training [DDS+09; KSL19] on classifiers trained for the WATERBIRDS task [SKH+20]. To study this, we compare two classes of ResNet-50 models trained with the exact same settings (see Appendix B) modulo the use of ImageNet pre-training, i.e.,

- **Algorithm A₁:** Pre-training on ImageNet, followed by full-network finetuning on WATERBIRDS. Models attain 89.1% average accuracy.
- **Algorithm A₂:** Training directly on WATERBIRDS. Models attain 63.9% average accuracy.

Identifying IDTs with MODELDIFF. We apply MODELDIFF just as in Section 4.1, with results shown in Figure 5. Verifying our results, we identify two candidate distinguishing features:

- **Yellow color:** Subpopulation A comprises test images that contain yellow birds belonging to class “landbird.” This leads us to hypothesize that models trained from scratch (i.e., without ImageNet pre-training) spuriously rely on the color yellow to predict the class “landbird,” whereas ImageNet-pretrained models do not. To test this hypothesis, we design a feature transformation that adds a yellow square patch to images (see Figure 6a).

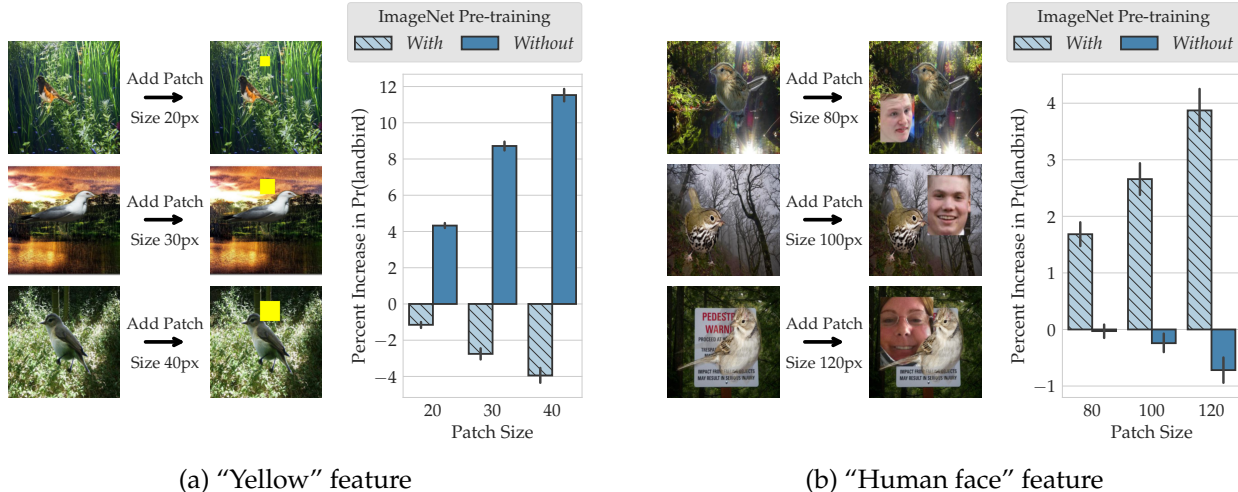


Figure 6: **Effect of ImageNet pre-training on WATERBIRDS classification.** Analogously to Figure 4, we use our framework to identify spurious correlations that are either suppressed or amplified by ImageNet pre-training. **(Left)** Adding a yellow patch to images makes models trained without (with) pre-training, on average, 9% more (2% less) confident in predicting the label “landbird.” **(Right)** Adding human faces to image backgrounds makes models trained with (without) pre-training, on average, 3% (0%) more confident in predicting the label “landbird.” Again, in both cases, increasing the intensity of feature transformations widens the gap in treatment effect between the two model classes.

- **Human face:** Subpopulation **B** comprises “landbird” images with *faces* in the background. This suggests that ImageNet pre-training introduces a spurious dependence on human faces to predict the label “landbird.” To test this hypothesis, we design a feature transformation that inserts patches of human faces to WATERBIRDS image backgrounds (see Figure 6b).

Once again, additional analysis (Appendix D) supports these hypotheses.

In Figure 6, we compare the effect of the above feature transformations on models trained with and without ImageNet pre-training. The results confirm both of our hypotheses. Adding a small (40px) yellow square patch to test images increased $P(\text{“landbird”})$ by 12% for models trained from scratch but *decreased* $P(\text{“landbird”})$ for models pre-trained on ImageNet. Similarly, adding a human face patch⁴ to image backgrounds increased $P(\text{“landbird”})$ by up to 4% for pre-trained models, but did not significantly affect models trained from scratch. Once again, increasing the intensity (i.e., patch size) of these feature transformations further widens the gap in sensitivity between the two model classes.

Streamlining the verification step with CLIP. Since one can apply MODELDIFF across a variety of domains (i.e., anywhere where one can compute datamodels), we have left the verification step intentionally vague so far. However, often the structure of the data being studied allows us to find IDTs in a more streamlined manner. For example, in Appendix F.5 we apply CLIP [RKH+21] to generate automatically hypotheses for this case study. Given the images in subpopulations **A** and **B**, CLIP generates candidate captions {“yellow”, “canary”, “lemon”} and {“florists”, “florist”, “faces”} respectively (see Appendix F.5 for more details).

⁴We collect a bank of human face patches using ImageNet validation examples and their corresponding face annotation [YYF+22]; see Appendix B.4 for more information.

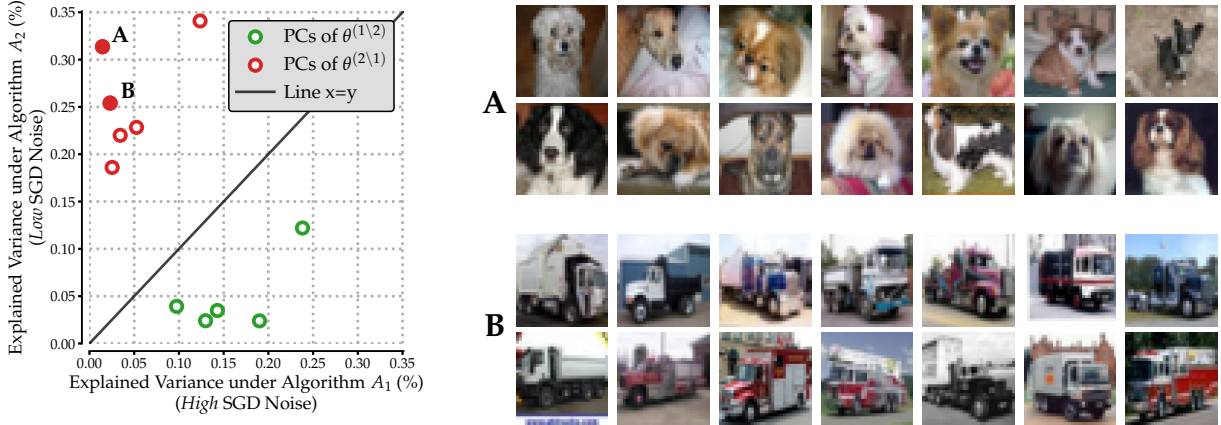


Figure 7: **Comparing CIFAR-10 models trained with high and low SGD noise.** An analog to Figure 3 for our third case study. Here, subpopulation **A** seems to correspond to dogs with a particular texture, and subpopulation **B** to front-facing trucks with a prominent rectangular shape.

Connections to prior work. Our results show that ImageNet pre-training reduces dependence on some spurious correlations (e.g., yellow color \rightarrow landbird) but also *introduces* new ones (e.g., human face \rightarrow landbird). These findings connect to the (seemingly contradictory) phenomenon where pre-training improves robustness to spurious features [GML22; TLG+20] while also transferring over spurious correlations [SJI+22; NSZ20] from the pre-training dataset.

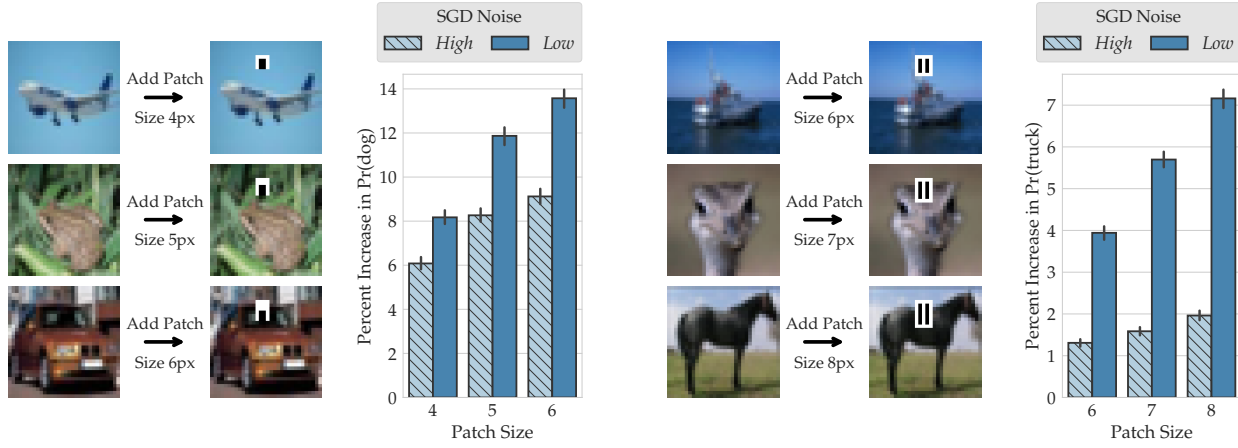
4.3 Case study: Optimizer hyperparameters

The choices of optimizer and corresponding hyperparameters can affect both the trainability and the generalization of resulting models [HHS17; KMN+17]. In this case study, we study the effect of two hyperparameters—learning rate and batch size—that control the effective scale of the noise in stochastic gradient descent (SGD). We study the effect of these hyperparameters in the context of CIFAR-10 [Kri09] classifiers by comparing the following two learning algorithms:

- **Algorithm A_1 :** Training with high SGD noise, i.e., large learning rate (0.1) and small batch size (256). Models attain 93% average test accuracy.
- **Algorithm A_2 :** Training with low SGD noise, i.e., small large rate (0.02) and large batch size (1024). Models attain 89% average test accuracy.

Identifying IDTs with MODELDIFF. We apply MODELDIFF just as in Section 4.1, with results shown in Figure 7.

- **Black-and-white texture:** Subpopulation **A** contains two-colored dogs (Figure 7, top right). The low-resolution nature of CIFAR-10 makes it difficult to identify a single distinguishing feature from this subpopulation. Additional analysis using datamodels (Appendix D), however, reveals a set of black-and-white training images from other classes that influence predictions on subpopulation **A** only when models are trained with low SGD noise (algorithm A_2). We thus hypothesize that models trained with low SGD noise rely more on black-and-white textural features to predict the class “dog.” To test this hypothesis, we design a transformation that adds a small black-and-white patch to a given image (see Figure 8a).



(a) "Black-and-white texture" feature

(b) "Rectangular shape" feature

Figure 8: **Effect of SGD hyperparameters on CIFAR-10 models.** Analogously to Figures 4 and 6, we use our framework to identify features that distinguish models trained with lower SGD noise from models trained with higher SGD noise. **(Left)** Adding a black-and-white patch to images makes models trained with low (high) SGD noise, on average, 11% (8%) more confident in predicting the label "dog." **(Right)** Adding high-contrast rectangles to images makes models trained with low (high) SGD noise, on average, 5.5% (1.5%) more confident in predicting the label "truck." In both cases, increasing the intensity of feature transformations widens the gap in treatment effect between the two model classes.

- **Rectangular shape:** Direction **B** surfaces a subpopulation of front-facing trucks (Figure 7, bottom right) that all have a similar rectangularly-shaped cabin and cargo area. The same style of additional analysis (see Appendix D) supports this observation, and suggests that models trained with low SGD noise (i.e., with \mathcal{A}_2) rely on rectangular-shaped patterns to predict the class "truck". To test this hypothesis, we design a feature transformation that modifies a given image with a patch of two high-contrast rectangles, loosely resembling the cabin/cargo shape of trucks in the subpopulation **B** (see Figure 8b).

In Figure 8, we compare the effect of the above feature transformations on models trained with high and low SGD noise. The results again confirm both hypotheses. Adding a small (6px) black-and-white patch to test images increased $P(\text{"dog"})$ by 14% (9%) for models trained with low (high) SGD noise. Similarly, applying a small (8px) rectangular-shape patch increased $P(\text{"truck"})$ by 7% (2%) for models trained with low (high) SGD noise. Increasing the intensity (i.e., patch size) of the transformations again widens the gap in sensitivity between the two model classes.

Connections to prior work. This case study shows how reducing the scale of SGD noise can increase reliance on certain low-level features (e.g., rectangular shape \rightarrow trucks). While prior works show that lower SGD noise worsens aggregate model performance [KMN+17; WLG+19], our methodology identifies *specific* features that are amplified due to low SGD noise. Furthermore, the simplistic nature of the identified features corroborate the theoretical explanation put forth in Li et al. [LWM19]: learning rate scale determines the extent to which models memorize patterns that are easy-to-fit but hard-to-generalize. More broadly, our framework motivates a closer look at how features amplified via low SGD noise alter aggregate model performance.

5 Discussion

In this section, we discuss some ways of extending and evaluating MODELDIFF.

Adapting our framework for aggregate comparison. Our goal in this paper has been fine-grained feature-based comparisons between learning algorithms. This goal is different from the typical one studied in the *model comparison* literature [MBR+18; RGY+17; BNB21; DDS21; MRB18], where the objective is to quantify the similarity between two (fixed) models in aggregate. In Appendix F.1, we show how to use datamodels for this alternate objective.⁵ In short, we can use the cosine similarity between the two datamodels of an example x to measure how similarly training data impacts the two model classes’ predictions at x . Aggregating over all x then gives a distribution (which we can also summarize with a score) that quantifies the overall similarity of the two learning algorithms. We find that such a metric yields qualitatively accurate comparisons.

Alternative methods for inferring features from distinguishing subpopulations. Our case studies in Section 4 show that manual inspection of distinguishing subpopulations suffices to infer informative distinguishing transformations. More generally, we can supplement manual inspection with dataset-specific annotations [SF21] or domain-specific tools such as vision-language models. In Appendix F.5, we illustrate how using CLIP [RKH+21] can streamline feature extraction. Specifically, we leverage CLIP’s shared vision-language embedding space to identify candidate distinguishing features by generating captions (or, descriptions) that best describe distinguishing subpopulations. For problems in other domains, one could employ other domain-specific tools to assist with feature inference.

On prediction-level comparisons between two learning algorithms. MODELDIFF extracts distinguishing subpopulations by analyzing how training data influences test predictions. One might ask whether simply analyzing differences in predictions suffice to extract similar subpopulations. To investigate this, in Appendix F.4 we look at whether restricting our analysis to examples on which the predictions of the two learning algorithms agree affects the distinguishing directions that we identified in Section 4. Note that an analysis only based on disagreement in predictions trivially cannot identify any differences in this case. Our results indicate that MODELDIFF outputs similar distinguishing directions even in this case, suggesting that analyzing the role of training data allows MODELDIFF to extract finer-grained differences beyond just predictions.

Computational cost of datamodel estimation. The computational cost of MODELDIFF scales with the number of models trained to compute datamodels in the first step of our method. In Appendix F.3, we find that we can recover similar datamodels (and as a result, similar distinguishing subpopulations) even with $10\times$ fewer samples (i.e., number of models trained to estimate datamodels). More generally, the “black-box” usage of datamodels in our framework implies that any improvements to the sample efficiency of datamodel estimation would directly make MODELDIFF faster as well.

⁵Note, however, that by using datamodels we are comparing the two model classes rather than two fixed models.

6 Related work

Our case studies in Section 4 shed light on the implicit task-specific biases of various learning algorithms. We refer the reader to the “Connections to prior work” headings within each respective case study for a discussion of these biases. Here, we instead focus on placing our work into context with existing approaches to model and algorithm comparison in machine learning.

In particular, we compare and contrast our approach to algorithm comparison with approaches to the related problem of *model comparison*, where one tries to characterize the difference between two (usually fixed) machine learning models. For simple models (e.g., sparse linear), we can directly compare models in parameter space. However, distances between more complex models such as deep neural networks are much less meaningful. To this end, a long line of work has sought to design methods for characterizing the differences between models:

Representation-based comparison. A popular approach (particularly in the context of deep learning) is to compare models using their internal *representations*. Since the coordinates of these representations do not have a consistent interpretation, representation-based model comparison typically studies the degree to which different models’ representations can be aligned. Methods based this approach include canonical correlation analysis (CCA) and variants [RGY+17; MRB18; CKM+22], centered kernel alignment (CKA) [KNL+19], graph-based methods [LYC+15; CLH+21], and model stitching [CKM+21; BNB21]. Prior works have used these methods to compare wide and deep neural networks [NRK21]; vision transformers and convolutional networks [RUK+21]; pre-trained and trained-from-scratch models [NSZ20]; and different language models [WBS+20]. Though they are often useful, prior work shows that representation-based similarity measures are not always reliable for testing functional differences in models [DDS21]. Our approach to algorithm comparison differs from these methods in both objective and implementation:

- *Learning algorithms rather than fixed models:* Rather than focusing on a single fixed model, our goal in this paper is to compare the classes of models that result from a given learning algorithm. In particular, we aim to find only differences that arise from algorithmic design choices, and not those that arise from the (sometimes significant) variability in training across random seeds [ZGK+21].
- *Feature-based rather than similarity-based:* Methods such as CCA and CKA focus on outputting a single score that reflects the overall similarity between two models. On the other hand, the goal of our framework is to find fine-grained differences in model behavior. Still, in Appendix F.1 we show that we can also use our method for more global comparisons, for instance by computing the average cosine similarity of the datamodel vectors.
- *Model-agnostic:* Our framework is agnostic to type of model used and thus allows one to easily compare models across learning algorithms—our method extends even to learning algorithms that do not have explicit representations (e.g., decision trees and kernel methods).

Example-level comparisons. An alternative method for comparing models is to compare their predictions directly. For example, Zhong et al. [ZGK+21] compare predictions of small and large language models (on a per-example level) to find that larger models are not uniformly better across example. Similarly, Mania et al. [MMS+19] study the *agreement* between models, i.e., how often they output the same prediction on a per-example level. In another vein, Meding et al. [MBG+22] show that after removing impossible or trivial examples from test sets, different models exhibit more variations in their predictions. Our framework also studies instance-level predictions, but ultimately connects the results back to human-interpretable distinguishing features.

Comparing feature attributions. Finally, another line of work compares models in terms of how they use features at test time. In the presence of a known set of features one can compute feature importances (e.g., using SHAP [LL17]) and compare them across models [WWZ+22]. In cases where we do not have access to high-level features, we can use instance-level explanation methods such as saliency maps to highlight different parts of the input, but these methods generally do not help at distinguishing models [DS22]. Furthermore, multiple evaluation metrics [AGM+18; HEK+18; SJN21] indicate that common instance-specific feature attribution methods can fail at accurately highlighting features learned by the model.

7 Conclusion

We introduce a general framework for fine-grained comparison of any two learning algorithms. Specifically, our framework compares models trained using two different algorithms in terms of how the models *rely on training data* to make predictions. Through three case studies, we showcase the utility of our framework in pinpointing how three aspects of the standard training pipeline—data augmentation, pre-training, optimization hyperparameters—can shape model behavior.

8 Acknowledgements

Work supported in part by the NSF grants CCF-1553428 and CNS-1815221, and Open Philanthropy. This material is based upon work supported by the Defense Advanced Research Projects Agency (DARPA) under Contract No. HR001120C0015.

Research was sponsored by the United States Air Force Research Laboratory and the United States Air Force Artificial Intelligence Accelerator and was accomplished under Cooperative Agreement Number FA8750-19-2-1000. The views and conclusions contained in this document are those of the authors and should not be interpreted as representing the official policies, either expressed or implied, of the United States Air Force or the U.S. Government. The U.S. Government is authorized to reproduce and distribute reprints for Government purposes notwithstanding any copyright notation herein.

References

- [AGM+18] Julius Adebayo, Justin Gilmer, Michael Muelly, Ian Goodfellow, Moritz Hardt, and Been Kim. “Sanity checks for saliency maps”. In: *Neural Information Processing Systems (NeurIPS)*. 2018.
- [AYZ22] Abubakar Abid, Mert Yuksekogonul, and James Zou. “Meaningfully Debugging Model Mistakes using Conceptual Counterfactual Explanations”. In: *arXiv preprint arXiv:2106.12723*. 2022.
- [BBL22] Randall Balestriero, Leon Bottou, and Yann LeCun. “The effects of regularization and data augmentation are class dependent”. In: *arXiv preprint arXiv:2204.03632* (2022).
- [BNB21] Yamini Bansal, Preetum Nakkiran, and Boaz Barak. “Revisiting Model Stitching to Compare Neural Representations”. In: *Neural Information Processing Systems (NeurIPS)*. 2021.
- [BWW+21] Manel Baradad Jurjo, Jonas Wulff, Tongzhou Wang, Phillip Isola, and Antonio Torralba. “Learning to see by looking at noise”. In: *Advances in Neural Information Processing Systems* 34 (2021), pp. 2556–2569.
- [CKM+21] Adrian Csizsarik, Peter Korosi-Szabo, Akos Matszangosz, Gergely Papp, and Daniel Varga. “Similarity and Matching of Neural Network Representations”. In: *Neural Information Processing Systems (NeurIPS)*. 2021.
- [CKM+22] Tianyu Cui, Yogesh Kumar, Pekka Marttinen, and Samuel Kaski. “Deconfounded Representation Similarity for Comparison of Neural Networks”. In: *Advances in Neural Information Processing Systems (NeurIPS)*. 2022.
- [CLH+21] Zuohui Chen, Yao Lu, JinXuan Hu, Wen Yang, Qi Xuan, Zhen Wang, and Ziaoniu Yang. “Revisit Similarity of Neural Network Representations From Graph Perspective”. In: *arXiv preprint arXiv:2111.11165* (2021).
- [DDS+09] Jia Deng, Wei Dong, Richard Socher, Li-Jia Li, Kai Li, and Li Fei-Fei. “Imagenet: A large-scale hierarchical image database”. In: *Computer Vision and Pattern Recognition (CVPR)*. 2009.
- [DDS21] Frances Ding, Jean-Stanislas Denain, and Jacob Steinhardt. “Grounding Representation Similarity with Statistical Testing”. In: *Advances in Neural Information Processing Systems (NeurIPS)*. 2021.
- [DG17] Piotr Dabkowski and Yarin Gal. “Real time image saliency for black box classifiers”. In: *Neural Information Processing Systems (NeurIPS)*. 2017.
- [DHM+20] Alexander D’Amour, Katherine A. Heller, Dan Moldovan, Ben Adlam, Babak Alipanahi, Alex Beutel, Christina Chen, Jonathan Deaton, Jacob Eisenstein, Matthew D. Hoffman, Farhad Hormozdiari, Neil Houlsby, Shaobo Hou, Ghassen Jerfel, Alan Karthikesalingam, Mario Lucic, Yi-An Ma, Cory Y. McLean, Diana Mincu, Akinori Mitani, Andrea Montanari, Zachary Nado, Vivek Natarajan, Christopher Nielson, Thomas F. Osborne, Rajiv Raman, Kim Ramasamy, Rory Sayres, Jessica Schrouff, Martin Seneviratne, Shannon Sequeira, Harini Suresh, Victor Veitch, Max Vladymyrov, Xuezhi Wang, Kellie Webster, Steve Yadlowsky, Taedong Yun, Xiaohua Zhai, and D. Sculley. “Underspecification Presents Challenges for Credibility in Modern Machine Learning”. In: *Arxiv preprint arXiv:2011.03395*. 2020.

- [DS22] Jean-Stanislas Denain and Jacob Steinhardt. “Auditing Visualizations: Transparency Methods Struggle to Detect Anomalous Behavior”. In: *arXiv preprint arXiv:2206.13498* (2022).
- [EVS+22] Sabri Eyuboglu, Maya Varma, Khaled Saab, Jean-Benoit Delbrouck, Christopher Lee-Messer, Jared Dunnmon, James Zou, and Christopher Ré. “Domino: Discovering systematic errors with cross-modal embeddings”. In: *arXiv preprint arXiv:2203.14960* (2022).
- [FZ20] Vitaly Feldman and Chiyuan Zhang. “What Neural Networks Memorize and Why: Discovering the Long Tail via Influence Estimation”. In: *Advances in Neural Information Processing Systems (NeurIPS)*. Vol. 33. 2020, pp. 2881–2891.
- [GML22] Soumya Suvra Ghosal, Yifei Ming, and Yixuan Li. “Are Vision Transformers Robust to Spurious Correlations?” In: *arXiv preprint arXiv:2203.09125* (2022).
- [GRM+19] Robert Geirhos, Patricia Rubisch, Claudio Michaelis, Matthias Bethge, Felix A. Wichmann, and Wieland Brendel. “ImageNet-trained CNNs are biased towards texture; increasing shape bias improves accuracy and robustness.” In: *International Conference on Learning Representations (ICLR)*. 2019.
- [GWZ+19] Amirata Ghorbani, James Wexler, James Zou, and Been Kim. “Towards automatic concept-based explanations”. In: *arXiv preprint arXiv:1902.03129* (2019).
- [HCK20] Katherine Hermann, Ting Chen, and Simon Kornblith. “The Origins and Prevalence of Texture Bias in Convolutional Neural Networks”. In: *Advances in Neural Information Processing Systems*. 2020.
- [HEK+18] Sara Hooker, Dumitru Erhan, Pieter-Jan Kindermans, and Been Kim. “A benchmark for interpretability methods in deep neural networks”. In: *arXiv preprint arXiv:1806.10758* (2018).
- [HHS17] Elad Hoffer, Itay Hubara, and Daniel Soudry. “Train longer, generalize better: closing the generalization gap in large batch training of neural networks”. In: *Advances in Neural Information Processing Systems (NeurIPS)*. 2017.
- [HRR+11] Frank R Hampel, Elvezio M Ronchetti, Peter J Rousseeuw, and Werner A Stahel. *Robust statistics: the approach based on influence functions*. Vol. 196. John Wiley & Sons, 2011.
- [HZR+15] Kaiming He, Xiangyu Zhang, Shaoqing Ren, and Jian Sun. *Deep Residual Learning for Image Recognition*. 2015.
- [IPE+22] Andrew Ilyas, Sung Min Park, Logan Engstrom, Guillaume Leclerc, and Aleksander Madry. “Datamodels: Predicting Predictions from Training Data”. In: *International Conference on Machine Learning (ICML)*. 2022.
- [JLM+22] Saachi Jain, Hannah Lawrence, Ankur Moitra, and Aleksander Madry. “Distilling Model Failures as Directions in Latent Space”. In: *arXiv preprint arXiv:2206.14754* (2022).
- [JNB+21] Yiding Jiang, Vaishnavh Nagarajan, Christina Baek, and J. Zico Kolter. “Assessing Generalization of SGD via Disagreement”. In: *Arxiv preprint arXiv:2106.13799*. 2021.
- [KL17] Pang Wei Koh and Percy Liang. “Understanding Black-box Predictions via Influence Functions”. In: *International Conference on Machine Learning*. 2017.

- [KMN+17] Nitish Shirish Keskar, Dheevatsa Mudigere, Jorge Nocedal, Mikhail Smelyanskiy, and Ping Tak Peter Tang. “On Large-Batch Training for Deep Learning: Generalization Gap and Sharp Minima”. In: *International Conference on Learning Representations (ICLR)*. 2017.
- [KNL+19] Simon Kornblith, Mohammad Norouzi, Honglak Lee, and Geoffrey Hinton. “Similarity of Neural Network Representations Revisited”. In: *Proceedings of the 36th International Conference on Machine Learning (ICML)*. 2019.
- [Kri09] Alex Krizhevsky. “Learning Multiple Layers of Features from Tiny Images”. In: *Technical report*. 2009.
- [KSL19] Simon Kornblith, Jonathon Shlens, and Quoc V Le. “Do better imagenet models transfer better?”. In: *computer vision and pattern recognition (CVPR)*. 2019.
- [KWG+18] Been Kim, Martin Wattenberg, Justin Gilmer, Carrie Cai, James Wexler, Fernanda Viegas, et al. “Interpretability beyond feature attribution: Quantitative testing with concept activation vectors (tcav)”. In: *International conference on machine learning (ICML)*. 2018.
- [LIE+22] Guillaume Leclerc, Andrew Ilyas, Logan Engstrom, Sung Min Park, Hadi Salman, and Aleksander Madry. *ffcv*. <https://github.com/libffcv/ffcv/>. 2022.
- [LL17] Scott Lundberg and Su-In Lee. “A unified approach to interpreting model predictions”. In: *Neural Information Processing Systems (NeurIPS)*. 2017.
- [LSI+21] Guillaume Leclerc, Hadi Salman, Andrew Ilyas, Sai Vemprala, Logan Engstrom, Vibhav Vineet, Kai Xiao, Pengchuan Zhang, Shibani Santurkar, Greg Yang, et al. “3DB: A Framework for Debugging Computer Vision Models”. In: *arXiv preprint arXiv:2106.03805*. 2021.
- [LWM19] Yuanzhi Li, Colin Wei, and Tengyu Ma. “Towards Explaining the Regularization Effect of Initial Large Learning Rate in Training Neural Networks”. In: *Neural Information Processing Systems (NeurIPS)*. 2019.
- [LXL+22] Hong Liu, Sang Michael Xie, Zhiyuan Li, and Tengyu Ma. “Same Pre-training Loss, Better Downstream: Implicit Bias Matters for Language Models”. In: *arXiv preprint arXiv:2210.14199*. 2022.
- [LYC+15] Yixuan Li, Jason Yosinski, Jeff Clune, Hod Lipson, and John Hopcroft. “Convergent Learning: Do different neural networks learn the same representations?”. In: *Proceedings of the 1st International Workshop on Feature Extraction: Modern Questions and Challenges at NIPS 2015*. 2015.
- [MBG+22] Kristof Meding, Luca M. Schulze Buschoff, Robert Geirhos, and Felix A. Wichmann. “Trivial or Impossible — dichotomous data difficulty masks model differences (on ImageNet and beyond)”. In: *International Conference on Learning Representations (ICLR)*. 2022.
- [MBR+18] Ari S Morcos, David GT Barrett, Neil C Rabinowitz, and Matthew Botvinick. “On the Importance of Single Directions for Generalization”. In: *International Conference on Learning Representations (ICLR)*. 2018.
- [Mil95] George A Miller. “WordNet: a lexical database for English”. In: *Communications of the ACM* (1995).

- [MMS+19] Horia Mania, John Miller, Ludwig Schmidt, Moritz Hardt, and Benjamin Recht. “Model similarity mitigates test set overuse”. In: *Advances in Neural Information Processing Systems (NeurIPS)*. 2019, pp. 9993–10002.
- [MRB18] Ari Morcos, Maithra Raghu, and Samy Bengio. “Insights on representational similarity in neural networks with canonical correlation”. In: *Advances in Neural Information Processing Systems* 31 (2018).
- [NRK21] Thao Nguyen, Maithra Raghu, and Simon Kornblith. “Do Wide and Deep Networks Learn the Same Things? Uncovering How Neural Network Representations Vary with Width and Depth”. In: *International Conference on Learning Representations (ICLR)*. 2021.
- [NSZ20] Behnam Neyshabur, Hanie Sedghi, and Chiyuan Zhang. “What is being transferred in transfer learning?” In: *Advances in neural information processing systems* 33 (2020), pp. 512–523.
- [RDS+15] Olga Russakovsky, Jia Deng, Hao Su, Jonathan Krause, Sanjeev Satheesh, Sean Ma, Zhiheng Huang, Andrej Karpathy, Aditya Khosla, Michael Bernstein, Alexander C. Berg, and Li Fei-Fei. “ImageNet Large Scale Visual Recognition Challenge”. In: *International Journal of Computer Vision (IJCV)*. 2015.
- [RGY+17] Maithra Raghu, Justin Gilmer, Jason Yosinski, and Jascha Sohl-Dickstein. “SVCCA: Singular Vector Canonical Correlation Analysis for Deep Learning Dynamics and Interpretability”. In: *Advances in Neural Information Processing Systems*. 2017.
- [RKH+21] Alec Radford, Jong Wook Kim, Chris Hallacy, Aditya Ramesh, Gabriel Goh, Sandhini Agarwal, Girish Sastry, Amanda Askell, Pamela Mishkin, Jack Clark, et al. “Learning transferable visual models from natural language supervision”. In: *arXiv preprint arXiv:2103.00020*. 2021.
- [RSG16] Marco Tulio Ribeiro, Sameer Singh, and Carlos Guestrin. ““ Why should I trust you?” Explaining the predictions of any classifier”. In: *International Conference on Knowledge Discovery and Data Mining (KDD)*. 2016.
- [RUK+21] Maithra Raghu, Thomas Unterthiner, Simon Kornblith, Chiyuan Zhang, and Alexey Dosovitskiy. “Do Vision Transformers See Like Convolutional Neural Networks?” In: *Neural Information Processing Systems (NeurIPS)*. 2021.
- [SBG22] Ruoqi Shen, Sebastien Bubeck, and Suriya Gunasekar. “Data Augmentation as Feature Manipulation”. In: *International Conference on Machine Learning*. PMLR. 2022, pp. 19773–19808.
- [SF21] Sahil Singla and Soheil Feizi. “Salient ImageNet: How to discover spurious features in Deep Learning?” In: *International Conference on Learning Representations*. 2021.
- [SJI+22] Hadi Salman, Saachi Jain, Andrew Ilyas, Logan Engstrom, Eric Wong, and Aleksander Madry. “When does Bias Transfer in Transfer Learning?” In: *arXiv preprint arXiv:2207.02842*. 2022.
- [SJNI21] Harshay Shah, Prateek Jain, and Praneeth Netrapalli. “Do Input Gradients Highlight Discriminative Features?” In: *Advances in Neural Information Processing Systems* 34 (2021).

- [SKH+20] Shiori Sagawa, Pang Wei Koh, Tatsunori B. Hashimoto, and Percy Liang. “Distributionally Robust Neural Networks for Group Shifts: On the Importance of Regularization for Worst-Case Generalization”. In: *International Conference on Learning Representations*. 2020.
- [STM21] Shibani Santurkar, Dimitris Tsipras, and Aleksander Madry. “Breeds: Benchmarks for subpopulation shift”. In: *International Conference on Learning Representations (ICLR)*. 2021.
- [SVZ13] Karen Simonyan, Andrea Vedaldi, and Andrew Zisserman. “Deep inside convolutional networks: Visualising image classification models and saliency maps”. In: *arXiv preprint arXiv:1312.6034* (2013).
- [TLG+20] Lifu Tu, Garima Lalwani, Spandana Gella, and He He. “An empirical study on robustness to spurious correlations using pre-trained language models”. In: *Transactions of the Association for Computational Linguistics* 8 (2020), pp. 621–633.
- [WBS+20] John Wu, Yonatan Belinkov, Hassan Sajjad, Nadir Durrani, Fahim Dalvi, and James Glass. “Similarity Analysis of Contextual Word Representation Models”. In: *Proceedings of the 58th Annual Meeting of the Association for Computational Linguistics*. 2020.
- [WBW+11] Catherine Wah, Steve Branson, Peter Welinder, Pietro Perona, and Serge Belongie. “The caltech-ucsd birds-200-2011 dataset”. In: (2011).
- [WLG+19] Yeming Wen, Kevin Luk, Maxime Gazeau, Guodong Zhang, Harris Chan, and Jimmy Ba. “An empirical study of large-batch stochastic gradient descent with structured covariance noise”. In: *arXiv preprint arXiv:1902.08234* (2019).
- [WSM21] Eric Wong, Shibani Santurkar, and Aleksander Madry. “Leveraging Sparse Linear Layers for Debuggable Deep Networks”. In: *International Conference on Machine Learning (ICML)*. 2021.
- [WWZ+22] Junpeng Wang, Liang Wang, Yan Zheng, Chin-Chia Michael Yeh, and Shubham Jain and Wei Zhang. “Learning-From-Disagreement: A Model Comparison and Visual Analytics Framework”. In: *arXiv preprint arXiv:2201.07849* (2022).
- [XEI+20] Kai Xiao, Logan Engstrom, Andrew Ilyas, and Aleksander Madry. “Noise or signal: The role of image backgrounds in object recognition”. In: *arXiv preprint arXiv:2006.09994* (2020).
- [YYF+22] Kaiyu Yang, Jacqueline H Yau, Li Fei-Fei, Jia Deng, and Olga Russakovsky. “A study of face obfuscation in imagenet”. In: *International Conference on Machine Learning*. PMLR. 2022, pp. 25313–25330.
- [ZGK+21] Ruiqi Zhong, Dhruva Ghosh, Dan Klein, and Jacob Steinhardt. “Are Larger Pre-trained Language Models Uniformly Better? Comparing Performance at the Instance Level”. In: *Findings of the Association for Computational Linguistics (Findings of ACL)*. 2021.
- [ZLK+17] Bolei Zhou, Agata Lapedriza, Aditya Khosla, Aude Oliva, and Antonio Torralba. “Places: A 10 million image database for scene recognition”. In: *IEEE transactions on pattern analysis and machine intelligence*. 2017.

Appendices

A	Algorithm analysis	23
B	Experimental Setup	24
B.1	Datasets	24
B.2	Models, learning algorithms, and hyperparameters	24
B.3	Datamodels	25
B.4	Feature transformations	26
B.5	Training infrastructure	27
C	Additional related work	28
D	Additional analysis of distinguishing subpopulations	29
D.1	Case study: Standard data augmentation	30
D.2	Case study: ImageNet pre-training	31
D.3	Case study: SGD hyperparameters	32
E	Additional evaluation of feature transformations	34
E.1	Case study: Standard data augmentation	34
E.2	Case study: ImageNet pre-training	35
E.3	Case study: SGD hyperparameters	36
F	Miscellaneous results	37
F.1	Aggregate metric for algorithm comparison	37
F.2	Explained variance of residual datamodel principal components	38
F.3	Effect of sample size on datamodel estimation	39
F.4	Effect of prediction-level disagreement on distinguishing training directions	41
F.5	Leveraging CLIP to analyze distinguishing subpopulations	42
F.6	Subpopulations surfaced by principal components of residual datamodels	44

A Algorithm analysis

Here, we give a more formal version of Proposition 1. First, we need to define the sense in which a given learning algorithm is sensitive to up/down-weighting the training set according to a training direction $u \in \mathbb{R}^{|S|}$.

Sensitivity along a training direction. We consider the following probabilistic notion of sensitivity: we measure how $f(x, S')$ varies in expectation, if relative to some base distribution \mathcal{D}_0 over S' , we up/down weight the probability of each training example by its weight u_i .

More specifically, for \mathcal{D}_0 , we consider sampling S' uniformly, i.e., by choosing each element of the full training set S with probability $1/2$. Then, we consider the perturbed distribution \mathcal{D}_u where x_i is sampled with probability $(1 + u_i)/2$. Finally, we define the *sensitivity* of $f(x, \cdot)$ along u (or *u-sensitivity*) as:

$$f(x, \cdot)|_u = (\mathbb{E}_{S' \sim \mathcal{D}_u} f(x, S') - \mathbb{E}_{S' \sim \mathcal{D}_0} f(x, S'))^2$$

where we take the square as we are interested in the magnitude.

We now give the formal result connecting the explained variance gap in datamodels (which we empirically observed in our case studies in Section 4) to the above definition of sensitivity.

Proposition 1 (Formal version of Proposition 1). *Consider two learning algorithms \mathcal{A}_1 and \mathcal{A}_2 applied to a training set S and evaluated on a test set T . Assume that their datamodels $\theta_x^{(1)}$ and $\theta_x^{(2)}$ perfectly approximate the respective model outputs $f^{(1)}(x, \cdot)$ and $f^{(2)}(x, \cdot)$. Then, for a given training direction $u \in \mathbb{R}^{|S|}$, the explained variance gap*

$$\Delta(\mathbf{u}) = \|\Theta^{(1)}\mathbf{u}\|^2 - \|\Theta^{(2)}\mathbf{u}\|^2$$

is equal to the following quantity:

$$\sum_{x \in T} f^{(1)}(x, \cdot)|_u - \sum_{x \in T} f^{(2)}(x, \cdot)|_u$$

which is the difference in *u-sensitivity* of model outputs of algorithms \mathcal{A}_1 and \mathcal{A}_2 .

Proof. With our linear assumption and definition of sensitivity, the proof is almost immediate. First, under the linearity assumption, the sensitivity $f(x_i, \cdot)|_u$ just reduces to $(\theta_i \cdot u)^2$. It follows that the total sensitivity, $\sum_i f(x_i, \cdot)|_u$ is just $\sum_i (\theta_i \cdot u)^2$, from which the claim follows. \square

B Experimental Setup

In this section, we outline the experimental setup—datasets, models, training algorithms, hyperparameters, and datamodels—used for our case studies in Section 4.

B.1 Datasets

Living17. The Living17 dataset [STM21] is an ImageNet-derived dataset, where the task is to classify images belonging to 17 types of living organisms (e.g., salamander, bear, fox). Each Living17 class corresponds to an ImageNet superclass (i.e., a set of ImageNet classes aggregated using WordNet [Mil95]). Santurkar et al. [STM21] introduce Living17 as one of four benchmark to evaluate model robustness to realistic subpopulation shifts. In our case study, we study the effect of data augmentation using a variant of this dataset, wherein the training and test images belong to the same set of subpopulations (i.e., no subpopulation shift).

Waterbirds. The Waterbirds dataset [SKH+20] consists of bird images taken from the CUB dataset [WBW+11] and pasted on backgrounds from the Places dataset [ZLK+17]. The task here is to classify “waterbirds” and “landbirds” in the presence of spurious correlated “land” and “water” backgrounds in the training data. Sagawa et al. [SKH+20] introduce Waterbirds as a benchmark to evaluate models under subpopulation shifts induced by spurious correlations. In our case study, we compare how models trained from scratch on Waterbirds data differ from ImageNet-pretrained models that are fine-tuned on Waterbirds data.

CIFAR-10. We consider the standard CIFAR-10 [Kri09] image classification dataset in order to study the effect of two SGD hyperparameters: learning rate and batch size.

Summary statistics of the datasets described above are outlined in Table 1.

Table 1: Summary statistics of datasets

Dataset	Classes	Size (Train/Test)	Input Dimensions
Living17	17	88,400/3,400	$3 \times 224 \times 224$
Waterbirds	2	4,795/5,794	$3 \times 224 \times 224$
CIFAR-10	10	50,000/10,000	$3 \times 32 \times 32$

B.2 Models, learning algorithms, and hyperparameters

Living17. We use the standard ResNet18 architecture [HZR+15] from the torchvision library. We train models for 25 epochs using SGD with the following configuration: initial learning rate 0.6, batch size 1024, cyclic learning rate schedule (with peak at epoch 12), momentum 0.9, weight decay 0.0005, and label smoothing (with smoothing hyperparameter 0.1). To study the effect of data augmentation, we train models with the following algorithms:

- **Algorithm \mathcal{A}_1 (with data augmentation):** Models are trained with standard data augmentation: random resized cropping (with default torchvision hyperparameters) and random horizontal flips. On average, models attain 89.2% average test accuracy.
- **Algorithm \mathcal{A}_2 (without data augmentation):** Models are trained without data augmentation. On average, models attain 81.9% average test accuracy.

Waterbirds. We use the standard ResNet50 architecture from the `torchvision` library. We train models using SGD with momentum 0.9 and weight decay 0.0001 for a maximum of 50 epochs (and stop early if the training loss drops below 0.01). For model selection, we choose the model checkpoint that has the maximum average accuracy on the validation dataset. As in Sagawa et al. [SKH+20], we do not use data augmentation. In our case study on pre-training, we consider ImageNet pre-trained models from `torchvision`. We consider models trained using the following algorithms:

- **Algorithm \mathcal{A}_1 (ImageNet pre-training):** Models pre-trained on ImageNet are fully fine-tuned on Waterbirds data with a fixed SGD learning rate 0.005 and batch size 64. On average, models attain 89.1% (non-adjusted) average test accuracy and 63.9% worst-group test accuracy.
- **Algorithm \mathcal{A}_2 (Training from scratch):** Models are trained from scratch (i.e., random initialization) on Waterbirds data with SGD: initial learning rate 0.01, batch size 64, and a linear learning rate schedule ($0.2 \times$ every 15 epochs). On average, models attain 63.6% average test accuracy and 5.7% worst-group test accuracy.

CIFAR-10. We use the ResNet9 architecture from Kakao Brain⁶, which is optimized for fast training. We train models using SGD with momentum 0.9 and weight decay 0.0005 for a maximum of 100 epochs (and stop early if the training loss drops below 0.01). We augment training data with a standard data augmentation scheme: random resized cropping with 4px padding and random horizontal flips. To study the effect of SGD noise in our case study, we vary learning rate and batch size. Specifically, we compare models trained with the following algorithms:

- **Algorithm \mathcal{A}_1 (high SGD noise):** Models are trained with SGD using a large initial learning rate (0.1), small batch size (256), and a linear learning rate schedule ($0.5 \times$ every 20 epochs). On average, models attain 93.3% test accuracy.
- **Algorithm \mathcal{A}_2 (low SGD noise):** Models are trained with SGD using a small fixed learning rate (0.02) and large batch size (1024). On average, models attain 89.5% test accuracy.

B.3 Datamodels

Now, we provide additional details on datamodels which, we recall, are computed in the first step of our algorithm comparison framework.

Estimating linear datamodels. Recall that the datamodel vector for example x_j , $\theta_j^{(i)} \in \mathbb{R}^{|S|}$, encodes the importance of individual training examples S to model’s loss at example x_j when trained with algorithm \mathcal{A}_i . Concretely, given test example x_j and training set $S = \{x_1, \dots, x_d\}$, the datamodel θ_j is a sparse linear model (or surrogate function) trained on the following regression task: For a training subset $S' \subset S$, can we predict the correct-class margin $f_{\mathcal{A}}(x_j; S')$ of a model trained on S' with algorithm \mathcal{A} ? This task can be naturally formulated as the following supervised learning problem: Given a training set $\{(S_i, f_{\mathcal{A}}(x; S_i))\}_{i=1}^m$ of size m , the datamodel θ_j (for example x_j) is the solution to the following problem:

$$\theta_j = \min_{w \in \mathbb{R}^{|S|}} \frac{1}{m} \sum_{i=1}^m \left(w^\top \mathbf{1}_{S_i} - f_{\mathcal{A}}(x_j; S_i) \right)^2 + \lambda \|w\|_1, \quad (5)$$

⁶<https://github.com/wbaek/torchskelton/blob/master/bin/dawnbench/cifar10.py>

where $\mathbf{1}_{S_i}$ is a boolean vector that indicates whether examples in the training dataset $x \in S$ belong to the training subset S_i . Note that each datamodel training point $(S_i, f_{\mathcal{A}}(x_j, S_i))$ is obtained by (a) training a model f (e.g., ResNet9) on a subset of data S_i (e.g., randomly subsampled CIFAR data) and (b) evaluating the trained model’s output on example x_j . Algorithm 1 provides pseudocode for estimating datamodels:

Algorithm 1 An outline of the datamodeling framework introduced in [IPE+22].

```

1: procedure ESTIMATEDATAMODEL(target example  $x$ , train set  $S$  of size  $d$ , subsampling frac.
    $\alpha \in (0, 1)$ )
2:    $T \leftarrow []$  ▷ Initialize datamodel training set
3:   for  $i \in \{1, \dots, m\}$  do
4:     Sample a subset  $S_i \subset S$  from  $\mathcal{D}_S$  where  $|S_i| = \alpha \cdot d$ 
5:      $y_i \leftarrow f_{\mathcal{A}}(x; S_i)$  ▷ Train a model on  $S_i$  using  $\mathcal{A}$ , evaluate on  $x$ 
6:     Define  $\mathbf{1}_{S_i} \in \{0, 1\}^d$  as  $(\mathbf{1}_{S_i})_j = 1$  if  $x_j \in S_i$  else 0
7:      $T \leftarrow T + [(\mathbf{1}_{S_i}, y_i)]$  ▷ Update datamodel training set
8:    $\theta \leftarrow \text{RUNREGRESSION}(T)$  ▷ Predict the  $y_i$  from the  $\mathbf{1}_{S_i}$  vectors
9:   return  $\theta$  ▷ Result: a weight vector  $\theta \in \mathbb{R}^d$ 

```

Datamodel estimation hyperparameters. Recall that our algorithm comparison framework in Section 3 involves estimating two sets of datamodels $\{\theta^{(1)}\}$ and $\{\theta^{(2)}\}$ for learning algorithms \mathcal{A}_1 and \mathcal{A}_2 respectively. In our case studies, we estimate two datamodels, $\theta_i^{(1)}$ and $\theta_i^{(2)}$ for every example x_i in the test dataset. Estimating these datamodels entail three design choices:

- **Sampling scheme for train subsets:** Like in Ilyas et al. [IPE+22], we use α -random subsets of the training data, where α denotes the subsampling fraction; we set $\alpha = 50\%$ as it maximizes sample efficiency (or model reuse) for empirical influence estimation [FZ20], which is equivalent to a variant of linear datamodels [IPE+22].
- **Sample size for datamodel estimation:** Recall that a datamodel training set of size m corresponds to training m models (e.g., m ResNet18 models on CIFAR-10) on independently sampled train subsets (or masks). We estimate datamodels on LIVING17, WATERBIRDS, and CIFAR-10 using 120k, 50k, and 50k samples (or models) per learning algorithm respectively; we make a 90 – 10% train-validation split.
- **ℓ_1 sparsity regularization:** We use cross-validation to select the sparsity regularization parameter λ . Specifically, for each datamodel, we evaluate the MSE on a validation split to search over $k = 50$ logarithmically spaced values for λ along the regularization path. As in [IPE+22], we then re-compute the datamodel on the entire dataset with the optimal λ value and all m training examples.

B.4 Feature transformations

We counterfactually verify distinguishing feature candidates (inferred from distinguishing sub-populations) by evaluating whether the corresponding transformations change model behavior as hypothesized. Here, we describe the feature transformations used in Section 4 in more detail⁷.

⁷The code for these feature transformations is available at <https://github.com/MadryLab/modeldiff>.

Designing feature transformations. We design feature transformations that modify examples by adding a specific patch or perturbation. We vary the intensity of patch-based and perturbation-based transformations via patch size k and perturbation intensity δ respectively. Additional details specific to each case study:

- **Pre-training.** We use patch-based transformations in this case. For the yellow color feature, we add a $k \times k$ square yellow patch to the input. For the human face feature, we add a $k \times k$ image of a human face to the input. To avoid occlusion with objects in the image foreground, we add the human face patch to the background. We make a bank of roughly 300 human faces using ImageNet face annotations [YYF+22] by (a) cropping out human faces from ImageNet validation examples and (b) manually removing mislabeled, low-resolution, and unclear human face images.
- **Data augmentation.** We design perturbation-based transformations to verify the identified distinguishing features: spider web and polka dots. In both cases, we δ -perturb each input with a random crop of a fixed grayscale spider web or yellow polka dot pattern.
- **SGD hyperparameters.** We use patch-based transformations in this case study. For the black-white texture feature, we add a k -sized patch that loosely resembles a black-white dog nose. Similarly, for the rectangular shape feature, we add a k -sized patch that loosely resembles windows.

Evaluating feature transformations. As shown in Section 4, given two learning algorithms \mathcal{A}_1 and \mathcal{A}_2 , we evaluate whether a feature transformation F changes predictions of models trained with \mathcal{A}_1 and \mathcal{A}_2 as hypothesized. To evaluate the counterfactual effect of transformation F on model M , we evaluate the extent to which applying F to input examples x increases the confidence of models in a particular class y . In our experiments, we estimate this counterfactual effect by averaging over all test examples and over 500 models trained with each learning algorithm.

B.5 Training infrastructure

Data loading. We use FFCV⁸ [LIE+22], which removes the data loading bottleneck for smaller models, gives a 3-4 \times improvement in throughput (i.e., number of models a day per GPU).

Datamodels regression. In addition to FFCV, we use the fast-l1 package⁹—a SAGA-based GPU solver for ℓ_1 -regularized regression—to parallelise datamodel estimation.

Computing resources. We train our models on a cluster of machines, each with 9 NVIDIA A100 or V100 GPUs and 96 CPU cores. We also use half-precision to increase training speed.

⁸Webpage: <http://ffcv.io>

⁹Github repository: https://github.com/MadryLab/fast_l1

C Additional related work

In the main paper, we focused our discussion of related work to those closely related to the problem of algorithm comparison. Here, we give discuss additional related work on interpretability and debugging of model biases.

Interpretability, explainability, and debugging. Our method hinges on the interpretability of the extracted subpopulation. A long line of prior work propose different interpretability and explainability methods for models.

Local explanation methods include saliency maps [SVZ13; DG17; AGM+18], surrogate models such as LIME [RSG16], and Shapley values [LL17]. Our method is similar to per-example based interpretability methods such as influence functions [KL17] in that our interpretation is based on data; however, our analysis differs from these priors methods in that it looks at entire subpopulations of inputs.

Global interpretability and debugging methods often leverage the rich latent space of neural networks in order to identify meaningful subpopulations or biases more automatically. Concept activation vectors and its variants [KWG+18; AYZ22; GWZ+19] help decompose model predictions into a set of concepts. Other recent works [EVS+22; JLM+22] leverage the recent cross-model representations along with simple models—mixture models and SVMs, respectively—to identify coherent subpopulations or slices. Other methods [WSM21; SF21] analyze the neurons of the penultimate layer of (adversarially robust) models to identify spurious features. Our framework can be viewed as leveraging a different embedding space, that of datamodel representations, to analyze model predictions.

Robustness to specific biases. In applying our framework across the three case studies, we identify a number of both known and unknown biases. A large body of previous work aims at finding and debugging these biases: Priors works investigate specific biases such as the role of texture [GRM+19] or backgrounds [XEI+20] by constructing new datasets. Leclerc et al. [LSI+21] automate many of these studies in the context of vision models with a render-based framework. Crucially, these works rely on having control over data generation and having candidate biases ahead of time. See the “Connections to prior work” within each case study in Section 4 for additional details.

D Additional analysis of distinguishing subpopulations

As outlined in Section 3, we analyze distinguishing subpopulations to infer (and test) distinguishing feature transformations. In this section, we present additional analysis in order to substantiate the distinguishing features inferred in each case study.

First, we describe two additional tools that we use to analyze subpopulations surfaced by principal components (PCs) of residual datamodels.

- **Class-specific visual inspection.** As shown in Section 4, the subpopulation of test examples whose datamodels have maximum projection onto PCs of residual datamodels largely belong to same class; these subpopulation mostly surface images from the same class. So, a simple-yet-effective way to identify *subpopulation-specific* distinguishing feature(s) is to just visually contrast the surfaced subpopulation from a set of randomly sampled examples that belong to the same class.
- **Relative influence of training examples.** Given a subset of test examples $S' \subset S$, can we identify a set of training examples $T' \subset T$ that strongly influence predictions on S' when models are trained with algorithm \mathcal{A}_1 but not when trained with \mathcal{A}_2 ? Given datamodel representations $\{\theta_i^{(1)}\}$ for \mathcal{A}_1 and $\{\theta_i^{(2)}\}$ for \mathcal{A}_2 , we apply a two-step (heuristic) approach identify training examples with high influence on \mathcal{A}_1 relative to \mathcal{A}_2 :
 - First, given learning algorithm \mathcal{A}_i and test subset S' , we estimate the aggregate (positive or negative) influence of training example x_k on subset S by taking the absolute sum over the corresponding datamodel weights: $\sum_{j \in S'} |\theta_{jk}^{(i)}|$.
 - Then, we take the absolute difference between the aggregate influence estimates of training example x_k using $\theta^{(1)}$ and $\theta^{(2)}$. This difference measures the *relative influence* of training example x_k on predictions of test subset S when models are trained with algorithm \mathcal{A}_1 instead of algorithm \mathcal{A}_2 .

In our analysis, we (a) identify training examples that have top-most relative influence estimates and then (b) visually contrast the subsets of test examples (one for each learning algorithm) that are most influenced by these training examples.

D.1 Case study: Standard data augmentation

Our case study on LIVING17 data in Section 4.1 shows that standard data augmentation can amplify co-occurrence bias (spider web) and texture bias (polka dots). We further substantiate these findings with relative influence analysis (Figure 9) and class-specific visual inspection (Figure 12).

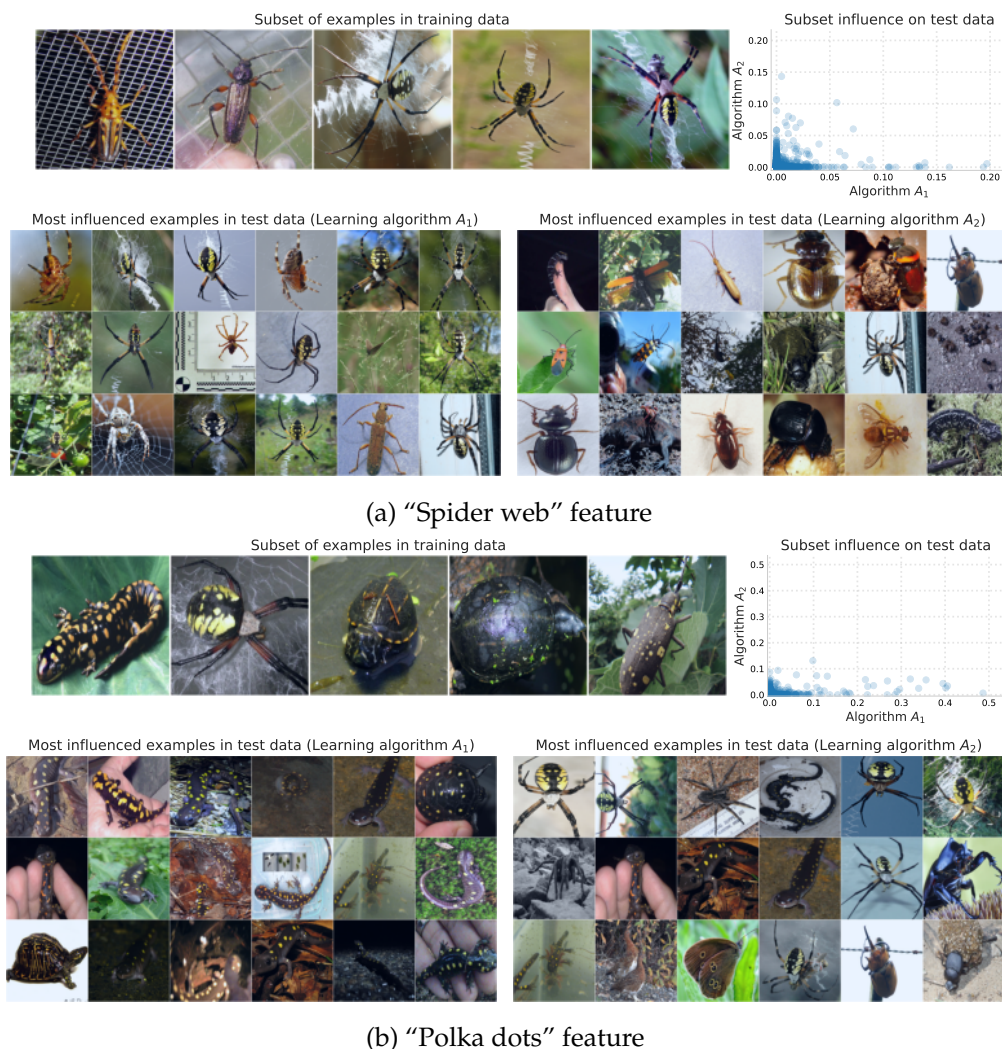


Figure 9: **Relative influence of training data on LIVING17 subpopulations.** Panel (a): Training images that contain web-like patterns have high relative influence on the “spider web” test subpopulation (see Figure 3). These images strongly influence model predictions on test images that contain spider webs (in bottom row) only when models are trained with augmentation (algorithm A_1). Panel (b): Training images that contain yellow-black texture have high relative influence on the “polka dots” test subpopulation (see Figure 3). These images strongly influence model predictions on test images of salamanders with yellow polka dots (in bottom row) only when models are trained with augmentation (algorithm A_1).

D.2 Case study: ImageNet pre-training

Our case study on WATERBIRDS data shows that ImageNet pre-training reduces dependence on the “yellow color” feature, but introduces dependence the “human face” feature. We support these findings with relative influence analysis in Figure 10 and additional inspection in Figure 13.

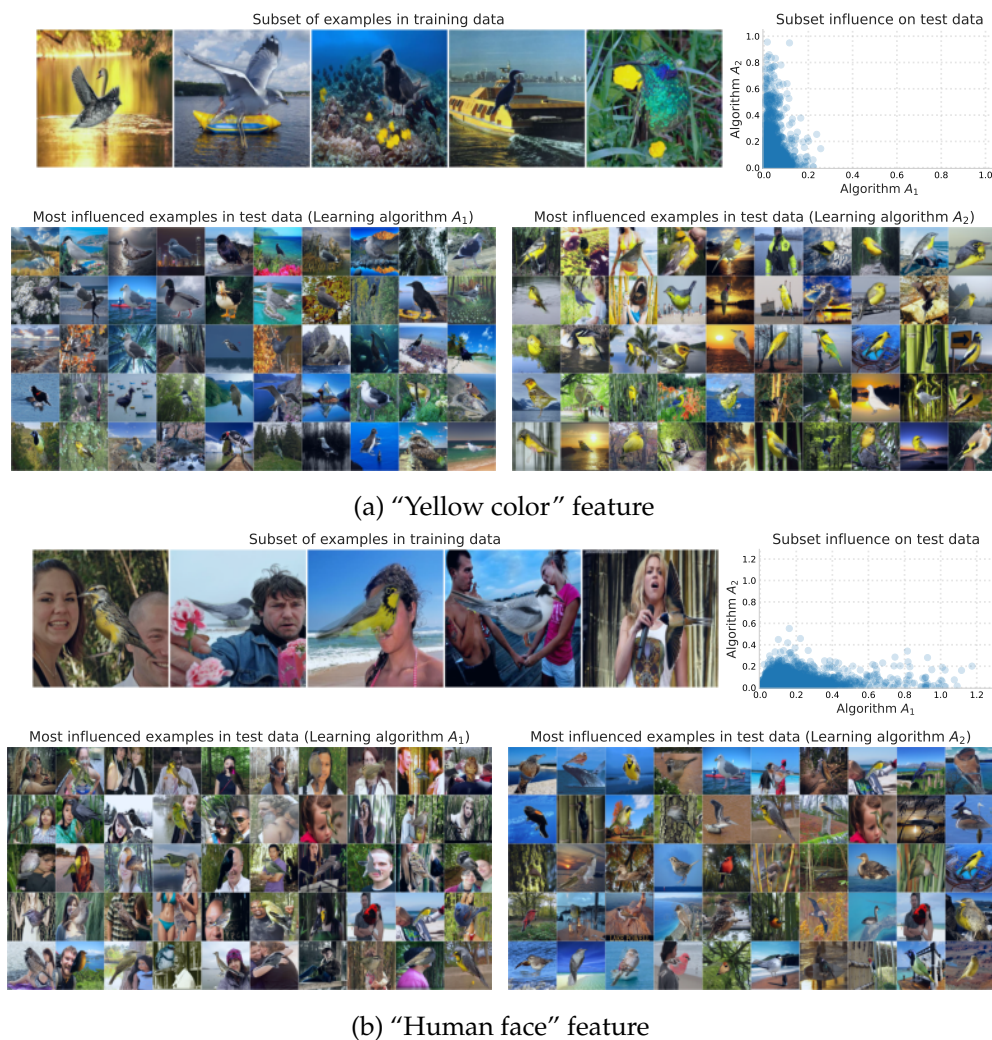


Figure 10: **Relative influence of training data on WATERBIRDS subpopulations.** Panel (a): Training images with yellow objects in the background have high relative influence on the “yellow color” test subpopulation (see Figure 5). These images strongly influence model predictions on test images that have yellow birds / objects (bottom row) only when models are trained from scratch (algorithm \mathcal{A}_2). Panel (b): Training images that contain human faces in the background have high relative influence on the “human face” test subpopulation (see Figure 5). These images strongly influence model predictions on test images (in bottom row) with human face(s) only when models are pre-trained on ImageNet (algorithm \mathcal{A}_1).

D.3 Case study: SGD hyperparameters

We analyze relative influence (Figure 11), and class-specific subpopulations (Figure 14) to hone in on two instances of distinguishing features—black-and-white texture and rectangular shape—in CIFAR-10 data that are amplified by low SGD noise.



Figure 11: **Relative influence of training data on CIFAR-10 subpopulations.** **Panel (a):** Training images with black-white objects have high relative influence on the “black-white” dog subpopulation (see Figure 7). These images influence model predictions on test images of black-white dogs (in bottom row) only when models are trained with low SGD noise (alg. A_2). **Panel (b):** Training images with high-contrast rectangular components in the background have high relative influence on the “rectangular shape” truck subpopulation (see Figure 7). These images influence model predictions on test images of front-facing trucks with prominent rectangular components (in bottom row) only when models are trained with low SGD noise (alg. A_2).

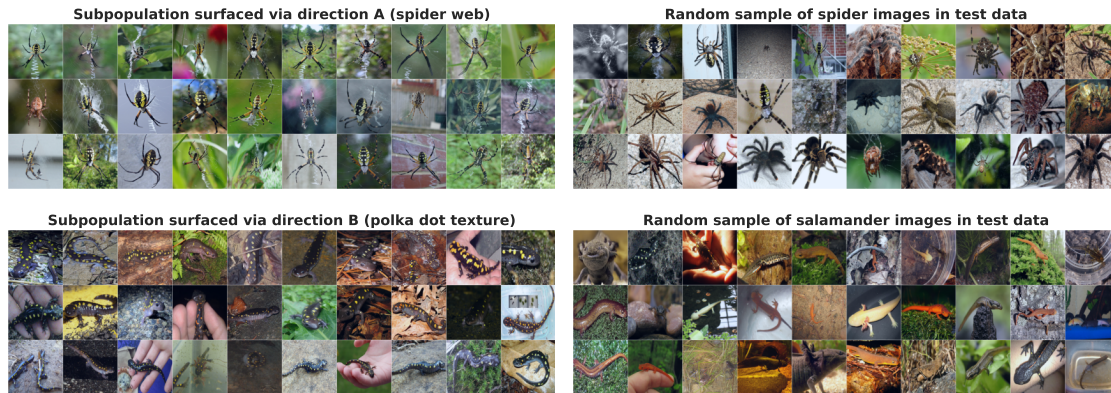


Figure 12: Class-specific visual inspection of LIVING17 subpopulations. **(Top)** In contrast to random LIVING17 images of spiders, the “spider web” subpopulation surfaces spiders with a prominent spider web in the background. **(Bottom)** Unlike random LIVING17 images of salamanders, the “polka dots” subpopulation surfaces salamanders that have a yellow-black polka dot texture.

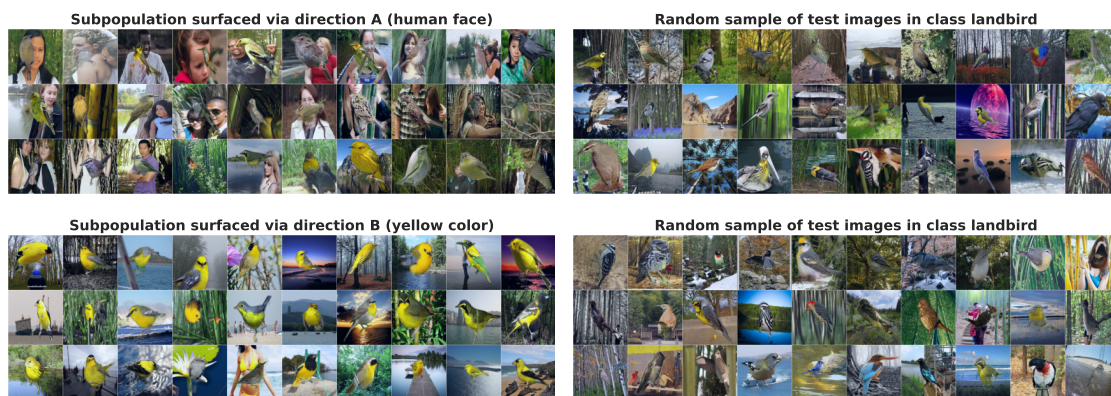


Figure 13: Class-specific visual inspection of WATERBIRDS subpopulations. **(Top)** In contrast to random “landbird” images, the “human face” subpopulation surfaces landbirds with human face(s) in the background. **(Bottom)** Unlike random “landbird” images, the “yellow color” subpopulation surfaces images with yellow birds *or* yellow objects in the background.



Figure 14: Class-specific visual inspection of CIFAR-10 subpopulations. In contrast to random images of dogs (top) and trucks (bottom), the “black-white” and “rectangular shape” subpopulations surface images of black-white dogs and front-facing trucks with multiple rectangular components respectively.

E Additional evaluation of feature transformations

Distinguishing feature transformations, which we recall from Section 3, are functions that, when applied to data points, change the predictions of one model class—but not the other—in a consistent way. In our case studies, we design distinguishing feature transformations that counterfactually verify features inferred from distinguishing subpopulations. Our findings in Section 4 use feature transformations to quantitatively measure the relative effect of the identified features on models trained with different learning algorithms. In this section, we present additional findings on feature transformations for each case study:

E.1 Case study: Standard data augmentation

In Section 4.1, we showed that standard data augmentation—horizontal flips and random crops—amplifies LIVING17 models’ reliance on “spider web” and “polka dots” to predict spiders and salamanders respectively. Figure 15 verifies our findings over a larger range of perturbation intensity δ values. We also observe that decreasing the minimum allowable crop size in `RandomResizedCrop` from 1.0 (i.e., no random cropping) to 0.08 (default `torchvision` hyperparameter) increases models’ sensitivity to both feature transformations.

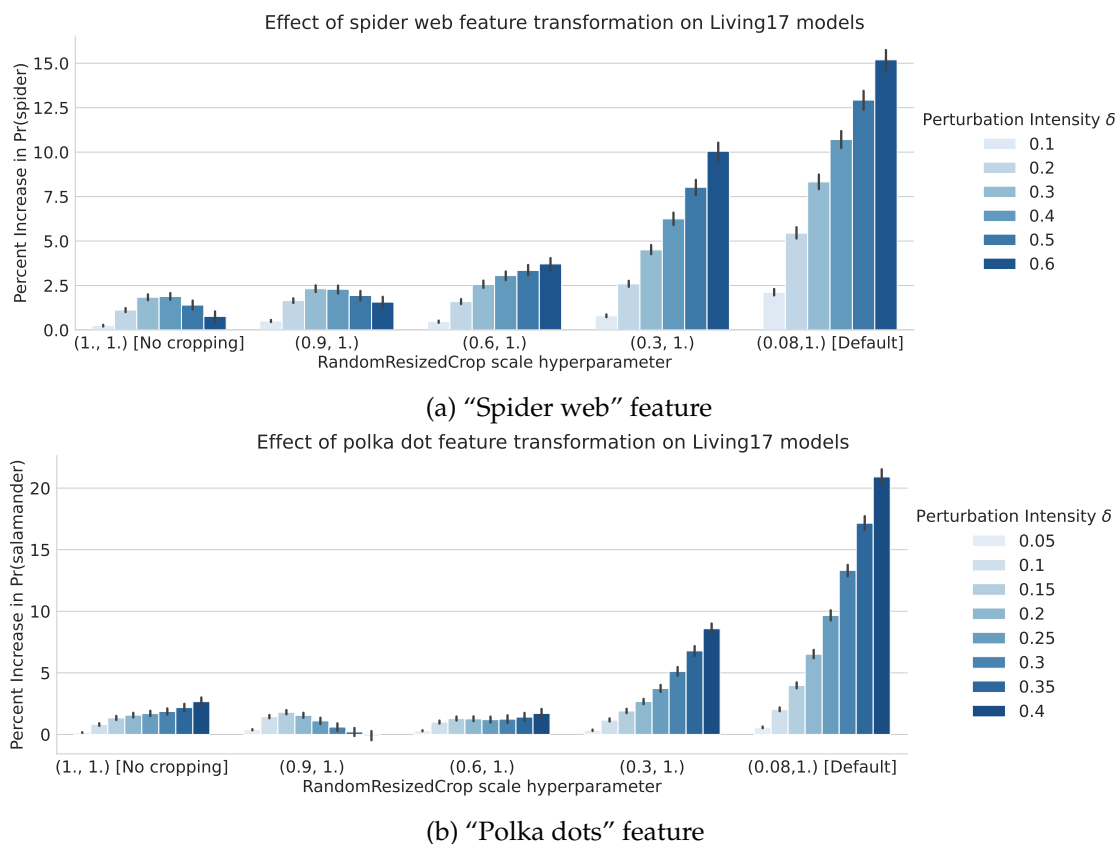


Figure 15: **Additional evaluation of LIVING17 feature transformations.** The top and bottom row evaluate the effect of “spider web” and “polka dot” feature transformations on models trained with different data augmentation schemes. Increasing the intensity of the transformations and the minimum crop size of `RandomResizedCrop` augmentation (via scale hyperparameter) increases the sensitivity of models to both feature transformations in a consistent manner.

E.2 Case study: ImageNet pre-training

In Section 4.2, we showed that fine-tuning ImageNet-pretrained ResNet50 models on WATERBIRDS data instead of training from scratch alters the relative importance of two spurious features: “yellow color” and “human face”. In Figure 16, we show that both feature transformations alter the predictions of ImageNet-pretrained ResNet18 and ImageNet-pretrained ResNet50 models in a similar way.

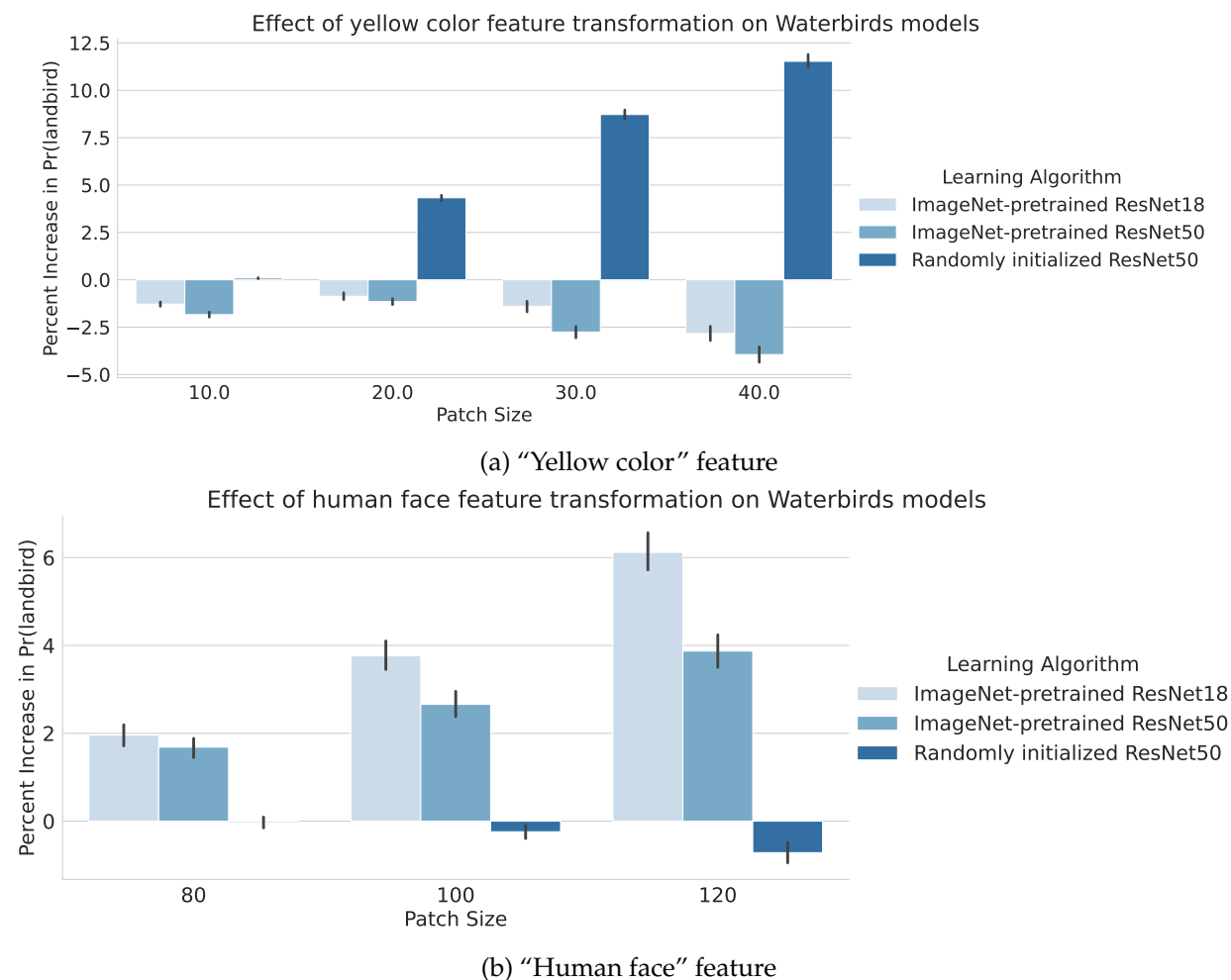
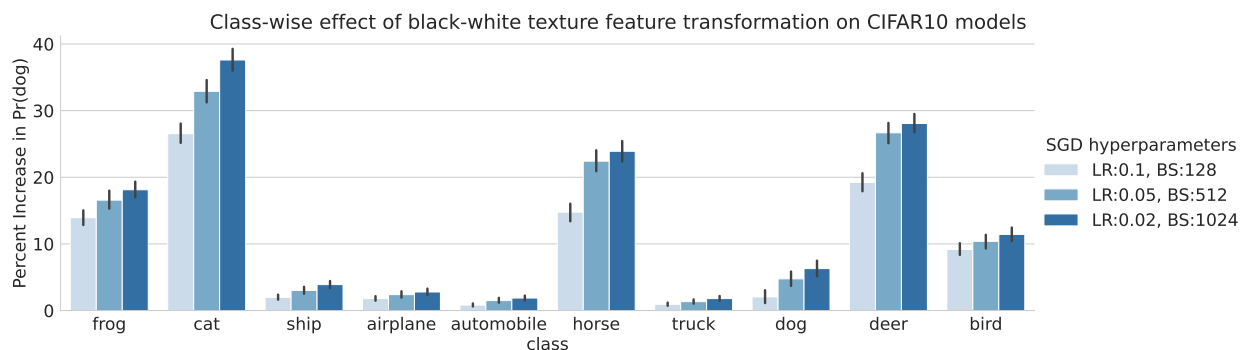


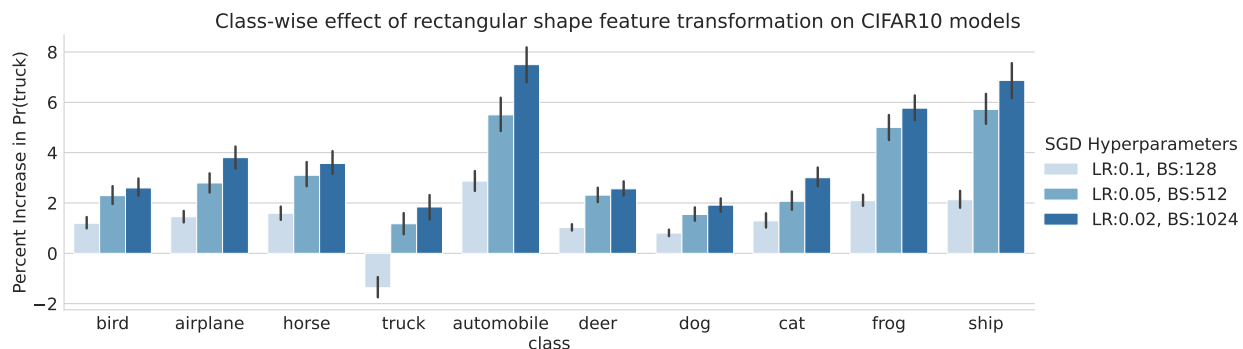
Figure 16: **Additional evaluation of WATERBIRDS feature transformations.** The top and bottom row evaluate the effect of “yellow color” and “human face” feature transformations on models trained with and without ImageNet pre-training. In both cases, unlike ResNet50 models trained from scratch, ImageNet-pretrained ResNet18 and ResNet50 models are sensitive to the “human face” transformation but not to the “yellow color” transformation.

E.3 Case study: SGD hyperparameters

In Section 4.3, we showed that reducing SGD noise results in CIFAR-10 models that are more sensitive to certain features, such as rectangular shape bias and black-white texture to predict trucks and dogs. In Figure 17, we evaluate how feature transformations change class-wise predictions of models trained with different SGD learning rate and batch size hyperparameters.



(a) "Black-white texture" feature



(b) "Rectangular shape" feature

Figure 17: **Additional evaluation of CIFAR-10 feature transformations.** The top and bottom row evaluate the effect of "black-white texture" and "rectangular shape" feature transformations on CIFAR-10 models trained with high (light blue), medium, and low (dark blue) SGD noise. In both cases, models trained with higher SGD noise are, on average, more sensitive to these transformations across all classes. Furthermore, the effect of the transformations are class-dependent—model predictions on transformed examples from semantically similar classes differ to a greater extent.

F Miscellaneous results

F.1 Aggregate metric for algorithm comparison

We can repurpose our framework as a similarity metric that quantifies the similarity of models trained with different learning algorithms in a more global manner. A straightforward approach to output a similarity score (or distribution) is to compute the cosine similarity of datamodel vectors. More concretely, let $\theta_i^{(1)}$ and $\theta_i^{(2)}$ denote the datamodels of example x_i with respect to models trained using learning algorithms \mathcal{A}_1 and \mathcal{A}_2 . Then, the cosine similarity between $\theta_i^{(1)}$ and $\theta_i^{(2)}$ measures the extent to which models trained with \mathcal{A}_1 and \mathcal{A}_2 depend on the same set of training examples to make predictions on example x_i .

We apply this metric to two case studies—pre-training (WATERBIRDS) and SGD noise (CIFAR-10)—in Figure 18. Specifically, Figure 18 plots the distribution of cosine similarity of datamodels for multiple learning algorithms over all test examples. The left subplot shows that on WATERBIRDS, ImageNet-pretrained ResNet50 models are, on average, more similar to ImageNet-pretrained ResNet18 models than to ResNet50 models pre-trained on synthetically generated data [BWW+21] and models trained from scratch. The right subplot shows that on CIFAR-10, ResNet9 models trained with high SGD noise are more similar to smaller-width ResNet9 models trained with high SGD noise than to ResNet9 models trained with low SGD noise.

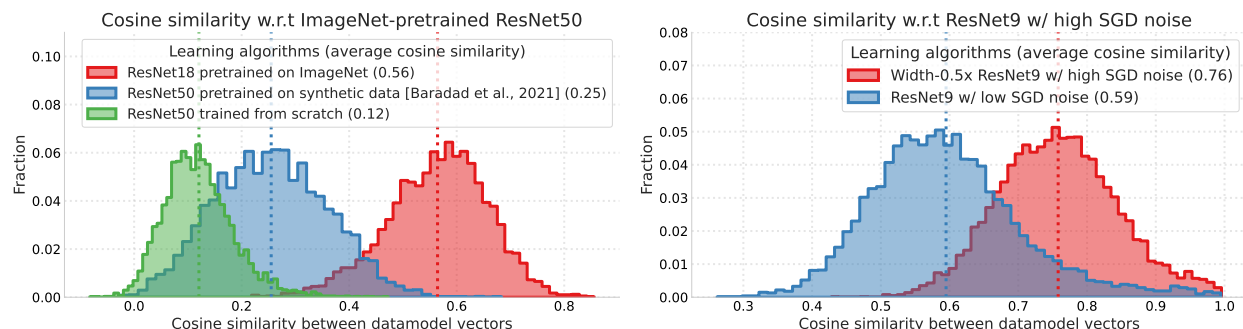


Figure 18: **Datamodel cosine similarity.** We use cosine similarity between two datamodel vectors as an aggregate metric to quantify the similarity of models trained with different learning algorithms. **(Left)** On WATERBIRDS data, datamodels of ImageNet-pretrained ResNet50 and ResNet18 models are more similar to each other than to models pre-trained on synthetically generated data and models trained from scratch. **(Right)** On CIFAR-10 data, ResNet models trained with high SGD noise are more similar to each other to ResNet models trained with low SGD noise.

F.2 Explained variance of residual datamodel principal components

Recall from Section 3 that the fraction of variance in datamodel representations $\{\theta_x^{(i)}\}$ explained by training direction v signifies the importance of the direction (or, combination of training examples) to predictions of models trained with algorithm \mathcal{A}_i . Through our case studies in Section 4, we show that the top 5 – 6 principal components (PCs) of residual datamodels $\theta^{(1\setminus 2)}$ correspond to training directions that have high explained w.r.t. datamodels of algorithm \mathcal{A}_1 but not \mathcal{A}_2 , and vice versa. Figure 19 shows that the top-100 PCs of residual datamodel $\theta^{(1\setminus 2)}$ (resp., $\theta^{(2\setminus 1)}$) have more (resp., less) explained variance on datamodel $\theta^{(1)}$ than on datamodel $\theta^{(2)}$.

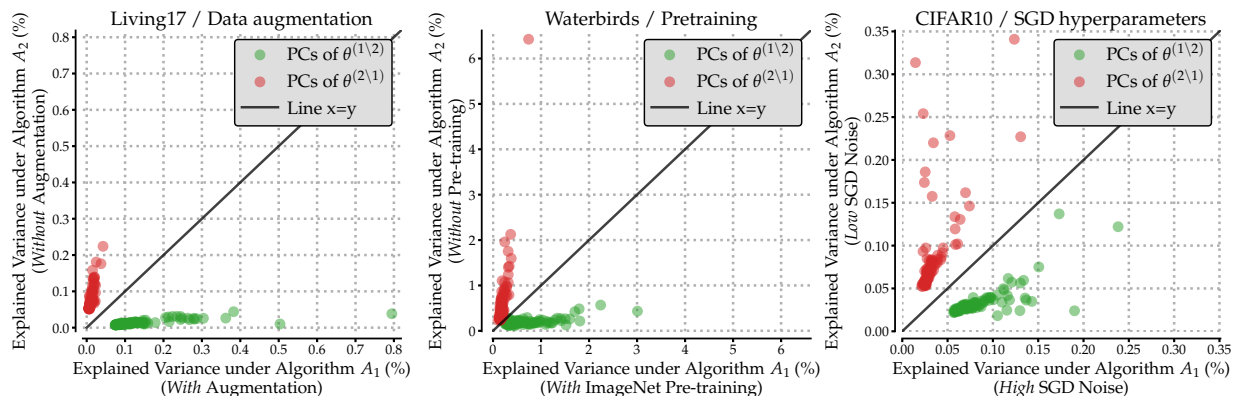


Figure 19: **Explained variance of residual datamodels’ principal components.** Highlighted in green (resp. red), the top-100 PCs of residual datamodel $\theta^{(1\setminus 2)}$ (resp. $\theta^{(2\setminus 1)}$) explain a larger (resp. smaller) fraction of datamodel variance under algorithm \mathcal{A}_1 than under algorithm \mathcal{A}_2 across all three case studies.

F.3 Effect of sample size on datamodel estimation

In this section, we analyze the effect of sample size on datamodel estimation.

Setup. Recall from Appendix B.3 that a datamodel training set of size m corresponds to training m models on independently sampled training data subsets. For our case study on ImageNet pre-training in Section 4.2, we estimate datamodels on WATERBIRDS data with 50,000 samples (i.e., m ResNet50 models trained on random subsets of the WATERBIRDS training dataset). In this experiment, we analyze how the estimated datamodels vary as a function of sample size $m \in \{5000, 10000, 25000, 50000\}$.

Cosine similarity between datamodels. Our algorithm comparisons framework uses normalized datamodel representations to compute distinguishing training directions in the first step. So, we first analyze the alignment between datamodel representations that are estimated with different sample sizes. Specifically, we evaluate the cosine similarity between $\theta_x^{(m_1)}$ and $\theta_x^{(m_2)}$, where vector $\theta_x^{(m)} \in \mathbb{R}^{|\mathcal{S}|}$ corresponds to the linear datamodel for example x estimated with m samples. As shown in Figure 20, the average cosine similarity between datamodels is greater than 0.9 even when the sample size is reduced by a factor of 10, from 50000 to 5000.

Explained variance of principal components. As discussed in Section 4, for a given training direction v , the fraction of variance that v explains in datamodel representations $\{\theta_x^{(i)}\}$ captures the importance of direction v (i.e., weighted combination of training examples) to the predictions of models trained using algorithm \mathcal{A}_i . Here, we show that principal components of datamodel representations trained with smaller sample size (e.g., $m = 5000$) have similar explained variance on datamodel representations estimated with larger sample size, and vice-versa. As shown in Figure 21, the explained variance of the top-10 principal components of datamodels estimated with $m \in \{5000, 50000\}$ have similar explained variance on datamodels estimated with $m \in \{5000, 10000, 25000, 50000\}$.

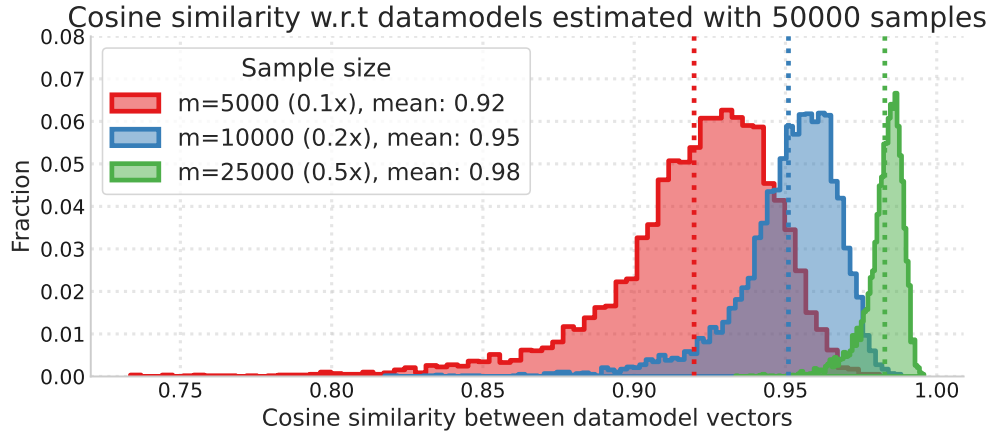


Figure 20: Histogram over cosine similarity between datamodels $\theta_x^{(m_1)}$ and $\theta_x^{(m_2)}$, where vector $\theta_x^{(m)} \in \mathbb{R}^{|\mathcal{S}|}$ corresponds to the linear datamodel for example x estimated with $m \in \{5000, 10000, 25000, 50000\}$ samples.

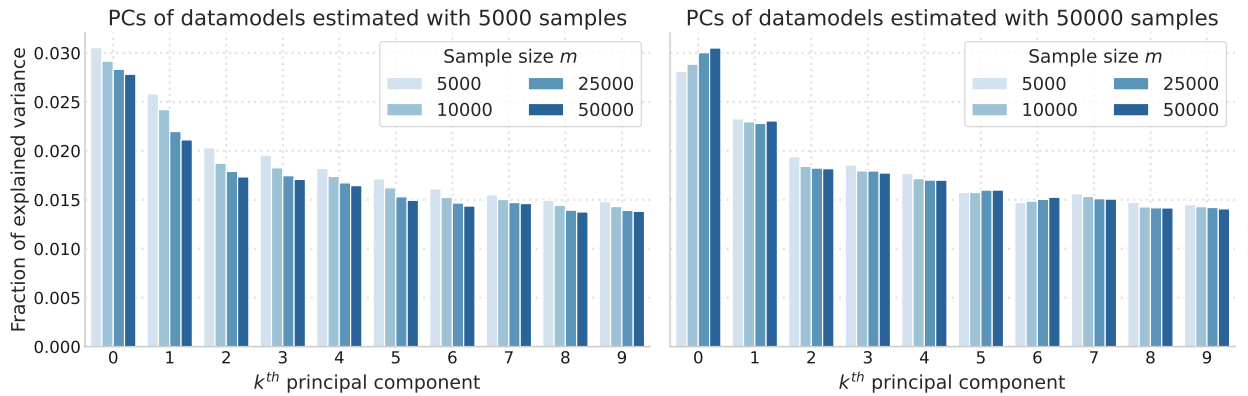


Figure 21: Explained variance of the top-10 principal components of datamodels estimated with $m \in \{5000, 50000\}$ have similar explained variance on datamodels estimated with sample size $m \in \{5000, 10000, 25000, 50000\}$.

F.4 Effect of prediction-level disagreement on distinguishing training directions

In this section, evaluate whether differences between algorithms at the model prediction level have a significant effect on the distinguishing training directions surfaced using our framework. For context, we note that there are no existing methods that analyze prediction-level differences for algorithm comparisons.

We design an experiment to show that example-level differences in predictions of models trained with different algorithms are not necessary to identify subpopulations analysed in our case studies. The first step of this experiment is to re-run our framework (a) on all test examples and (b) only on test examples on which models trained with different algorithm have the same prediction “mode” (taken over multiple runs). In the second step, we directly compare the alignment between distinguishing training directions before and after controlling for prediction-level differences.

Our results in Table 1 show that for each case study, our framework identifies similar training directions (i.e., high cosine similarity) even after removing test examples on which model predictions differ on average. This experiment shows that our framework can identify fine-grained differences between learning algorithms that persist even after controlling for prediction-level disagreement across models trained with different algorithms.

Dataset / Case study	Direction	(Absolute) Cosine Similarity
Living17 / Data augmentation	A (Spider web)	0.999
	B (Polka dots)	0.998
Waterbirds / ImageNet pre-training	A (Yellow color)	0.977
	B (Human face)	0.740
CIFAR-10 / SGD hyperparameters	A (Black-white texture)	0.998
	B (Rectangular shape)	0.999

Table 2: Distinguishing training directions obtained before and after filtering out high-disagreement test examples (a) exhibit high cosine similarity and (b) surface subpopulations of images that share the same distinguishing feature.

F.5 Leveraging CLIP to analyze distinguishing subpopulations

As discussed in Section 3 and Appendix D, we infer distinguishing features candidates through manual inspection of distinguishing subpopulations. In this section, we demonstrate that for image classifiers, shared vision-language models such as CLIP [RKH+21] provide a streamlined alternative to manual inspection of distinguishing subpopulations.

Approach. Before we describe our approach, note that CLIP is a contrastive learning method that embeds text and natural language into a shared embedding space. Our approach leverages CLIP embeddings to identify multiple *distinguishing captions*—representative descriptions that best contrast a given subpopulation of images from a set of images sampled from the same distribution. In the context of our framework, the CLIP-based approach takes as inputs a distinguishing training direction v , a set of images \mathcal{D} , and a set of captions \mathcal{S} ¹⁰, and outputs a set of distinguishing captions $\mathcal{S}' \in \mathcal{S}$ in four steps:

- *Pre-compute image and text embeddings.* Use the image encoder of a CLIP model to compute a set of normalized embeddings for all images in \mathcal{D} . Analogously, use the text encoder of a CLIP model to compute a set of normalized embeddings for all captions in \mathcal{S} .
- *Record image-text pairwise cosine similarity.* Let vector $C_i \in \mathcal{R}^{|\mathcal{S}|}$ denote the pairwise cosine similarity between the embedding of image $i \in \mathcal{D}$ and all captions $j \in \mathcal{S}$.
- *Compute mean cosine similarity over dataset and top- k subpopulation.* Compute the mean cosine similarity vector $\bar{C} = \frac{1}{n} \sum_{i \in \mathcal{D}} C_i$ over all images in \mathcal{D} . Similarly, given distinguishing training direction v , compute the mean cosine similarity vector $C^{(v)}$ over the top- k images whose residual datamodel vectors are most aligned with v .
- *Extract distinguishing captions \mathcal{S}' .* Use cosine similarity vectors \bar{C} and $C^{(v)}$ to extract captions in \mathcal{S} that have the maximum difference between $C_i^{(v)}$ and \bar{C}_i .

Intuitively, the set of distinguishing captions \mathcal{S}' correspond to representative captions (or, descriptions) that best contrast the top- k images surfaced by distinguishing direction v from the dataset.

Results. We now apply this approach to our case study on ImageNet pre-training, where we compare WATERBIRDS models trained with and without ImageNet pre-training (see Section 4). Specifically, we evaluate whether the CLIP-based approach surfaces distinguishing captions that are similar to distinguishing features “yellow color” (direction A) and “human face” (direction B) inferred via manual inspection. Figure 22 illustrates that for direction A), the CLIP-based approach highlights distinguishing captions such as yellow, lemon, and sulphur, all of which are similar to the “yellow color” feature that we infer via manual inspection. Similarly, Figure 23 shows that the distinguishing captions for direction B (e.g., florist, faces, counselors) are similar to the identified “human face” feature.

To summarize, we show how the verification step can be easily *specialized* to comparisons of vision classifiers trained on ImageNet-like data via vision-language embeddings such as CLIP.

¹⁰We use a filtered list of roughly 20,000 most common English words in order of frequency, taken from <https://github.com/first20hours/google-10000-english>.

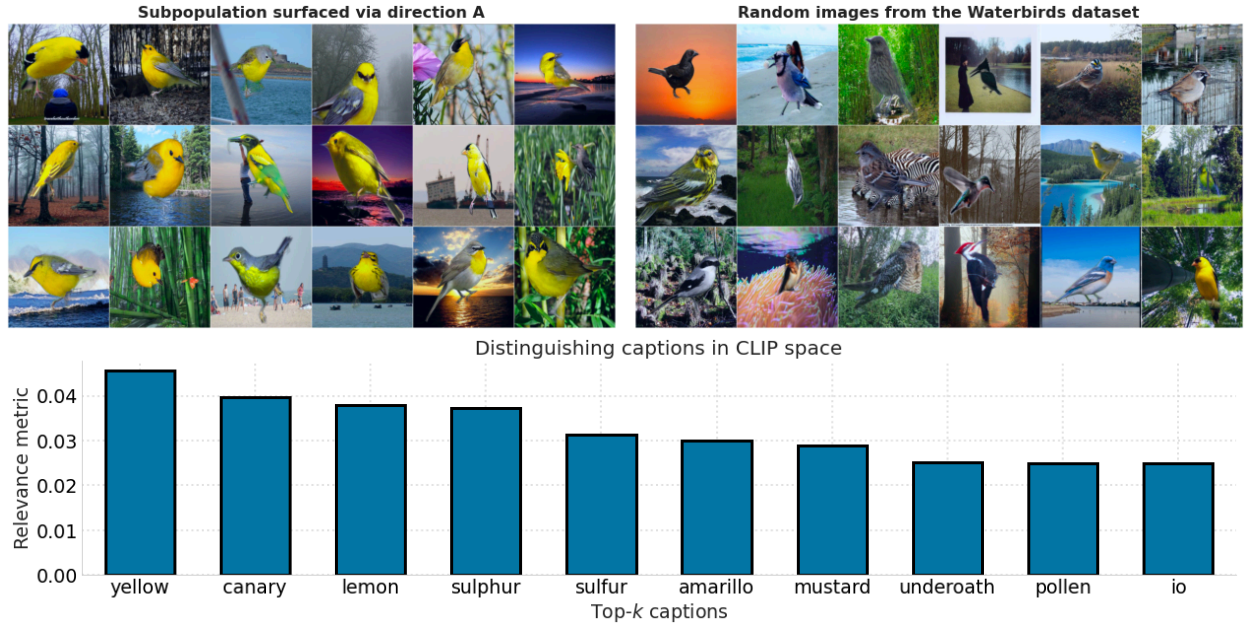


Figure 22: **Direction A.** The CLIP-based approach extracts distinguishing captions such as yellow, lemon, and sulphur, all of which contrast the residual subpopulation on the left to a set of random images from the WATERBIRDS dataset on the right. These distinguishing captions match the “yellow color” feature that we infer via manual inspection of the distinguishing subpopulation in Section 4.2.

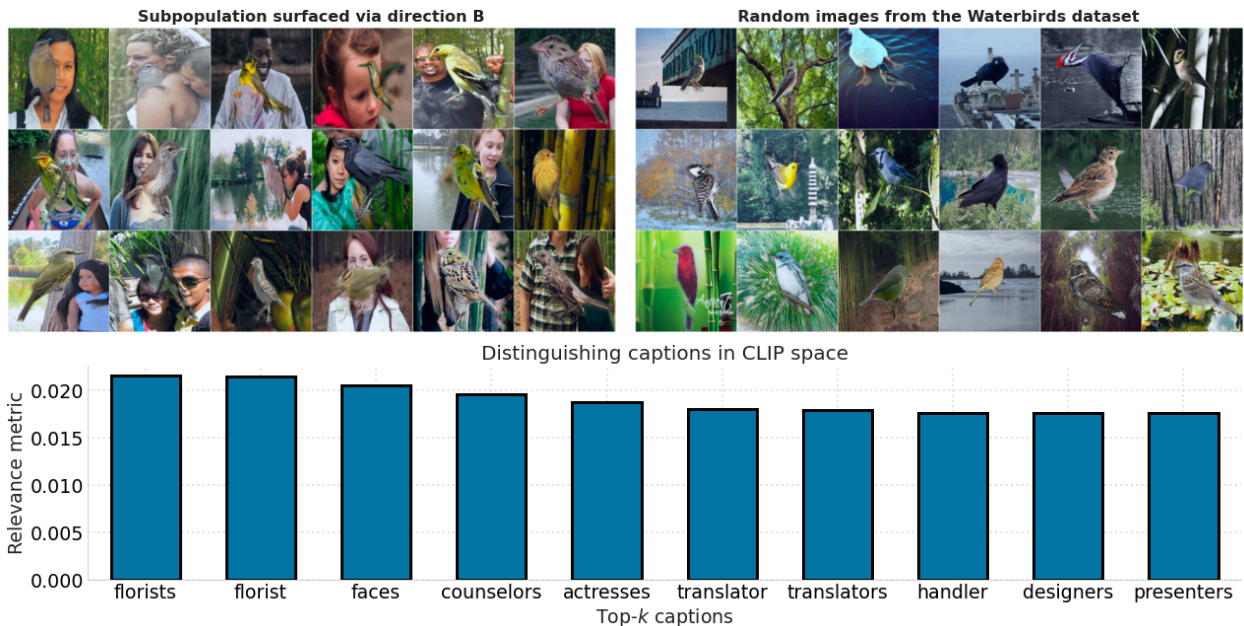


Figure 23: **Direction B.** The CLIP-based approach extracts distinguishing captions such as florists, faces, and counselors, all of which contrast the residual subpopulation (left) of images with human faces in the background to a set of random images (right) from the WATERBIRDS dataset. These distinguishing captions match the “human face” feature that we infer and counterfactually verify via manual inspection of the distinguishing subpopulation in Section 4.2.

E.6 Subpopulations surfaced by principal components of residual datamodels

Recall that our framework identifies distinguishing subpopulations via principal components (PCs) of residual datamodels. Specifically, these subpopulations correspond to test examples whose residual datamodel representations have the most positive (top- k) and most negative (bottom- k) projection onto a given PC. Here, we show that the top- k and bottom- k subpopulations corresponding to the top few PCs of residual datamodels considered in Section 4 surface test examples with qualitatively similar properties.

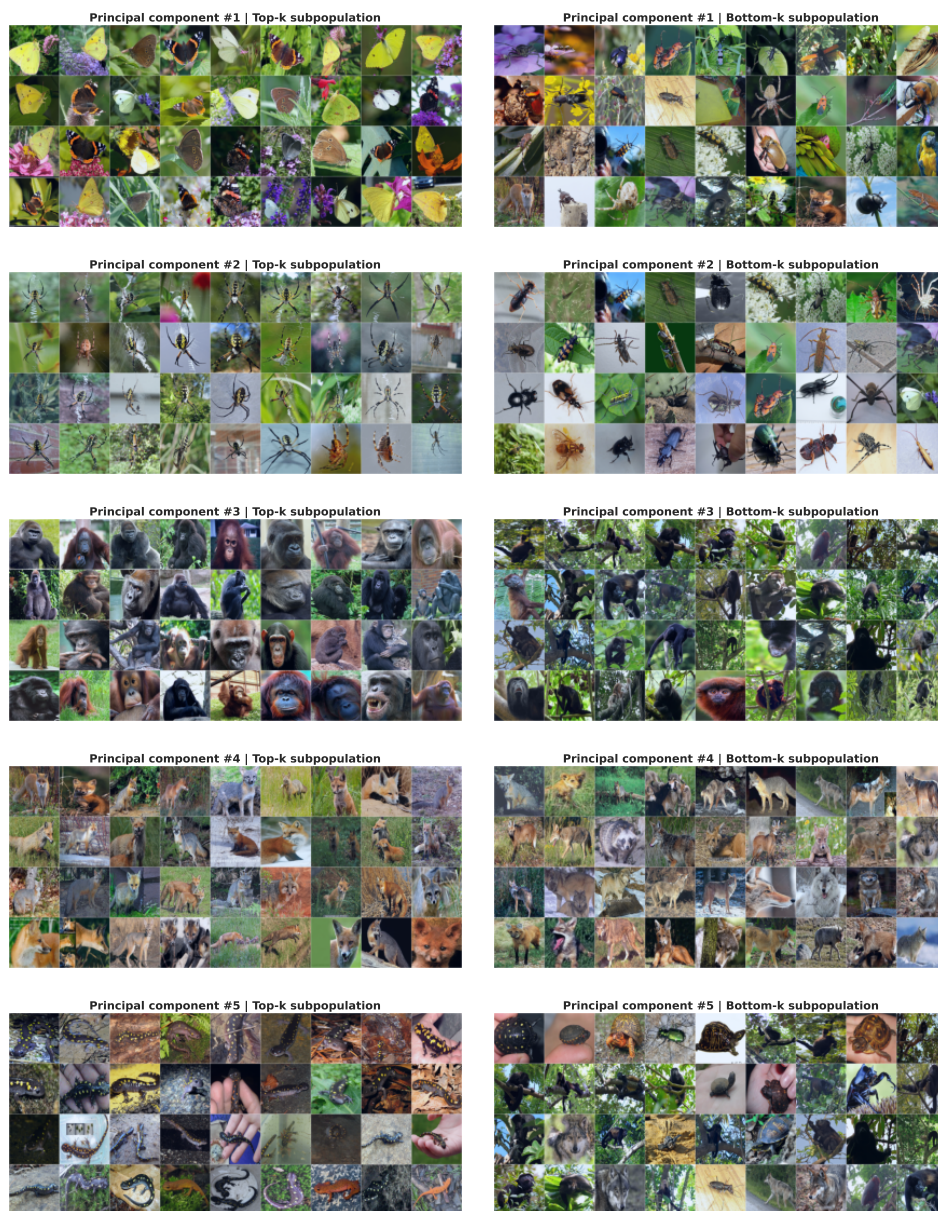


Figure 24: Top five PC subpopulations of LIVING17 residual datamodel $\theta^{(1\setminus 2)}$, where learning algorithms \mathcal{A}_1 and \mathcal{A}_2 correspond to training models with and without standard data augmentation respectively. Our case study in Section 4.1 analyzes PC #2 (direction **A**) and PC #5 (direction **B**).

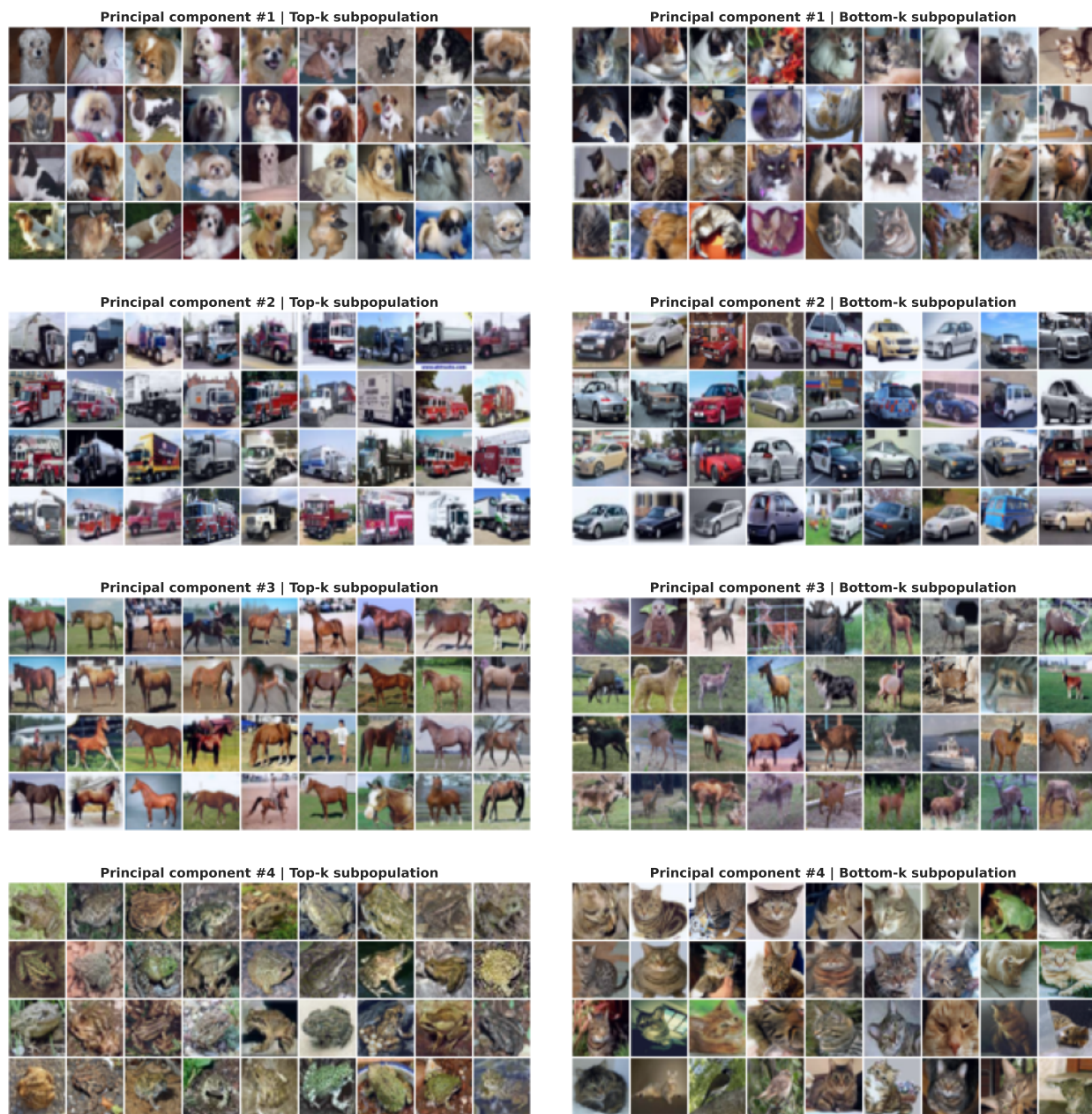


Figure 25: Top four PC subpopulations of CIFAR-10 residual datamodel $\theta^{(2\setminus 1)}$, where learning algorithms \mathcal{A}_1 and \mathcal{A}_2 correspond to training models with high and low SGD noise respectively. Our case study in Section 4.3 analyzes PC #1 (direction A) and PC #2 (direction B).



Figure 26: Top four PC subpopulations of WATERBIRDS residual datamodel $\theta^{(1\setminus 2)}$, where learning algorithms \mathcal{A}_1 and \mathcal{A}_2 correspond to training models with and without ImageNet pre-training respectively. Our case study in Section 4.1 analyzes PC #3 (direction A).

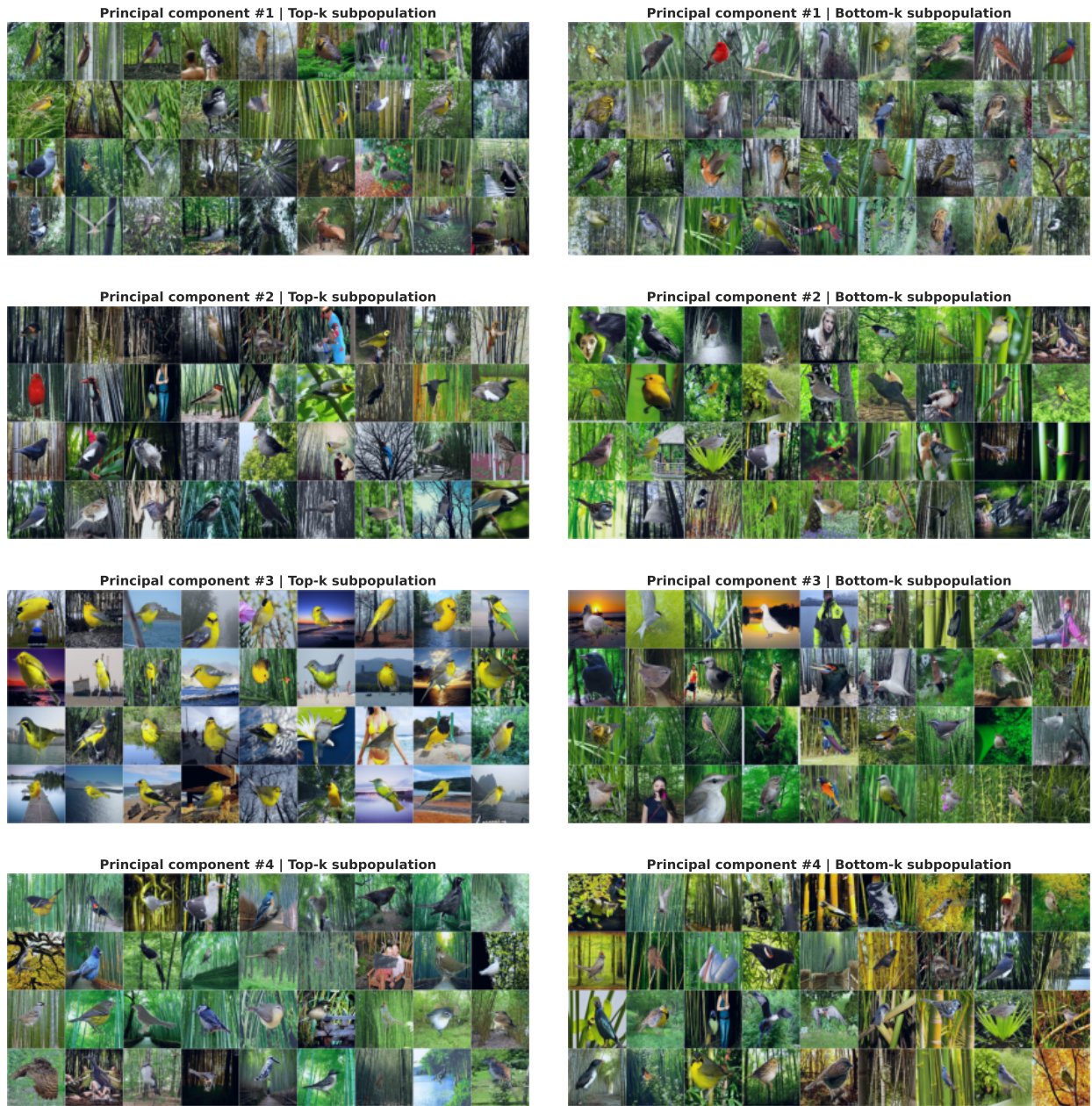


Figure 27: Top four PC subpopulations of WATERBIRDS residual datamodel $\theta^{(2\setminus 1)}$, where learning algorithms \mathcal{A}_1 and \mathcal{A}_2 correspond to training models with and without ImageNet pre-training respectively. Our case study in Section 4.1 analyzes PC #3 (direction **B**).